Title

Effects of LiDAR-derived, spatially distributed vegetation roughness on two-dimensional hydraulics in a gravel-cobble river at flows of 0.2 to 20 times bankfull

Journal

Geomorphology, 206

ISSN

0169555X

Authors

Abu-Aly, T.R.
Pasternack, G.B.
Wyrick, J.R.
et al.

Publication Date

2014-02-01

DOI

10.1016/j.geomorph.2013.10.017

Peer reviewed

Effects of LiDAR-derived, spatially distributed vegetation roughness on two-dimensional hydraulics in a gravel-cobble river at flows of 0.2 to 20 times bankfull

T. R. Abu-Aly[a], G.B. Pasternack[a]*, J.R. Wyrick[a], R. Barker[a], D. Massa[b], T. Johnson[b]

[a]Department of Land, Air, and Water Resources, University of California, One Shields Avenue, Davis, CA 95616-8626, USA

[b]Lower Yuba River Accord River Management Team, Marysville, CA 95901, USA

***Corresponding author. Tel.: +1 530 302-5658; Fax: +1 530 752-1552; E-mail: gpast@ucdavis.edu.**

Abstract

The spatially distributed effects of riparian vegetation on fluvial hydrodynamics during low flows to large floods are poorly documented. Drawing on a LiDAR-derived, meter-scale resolution raster of vegetation canopy height as well as an existing algorithm to spatially distribute stage-dependent channel roughness, this study developed a meter-scale two-dimensional hydrodynamic model of ~ 28.3 km of a gravel/cobble-bed river corridor for flows ranging from 0.2-20 times bankfull discharge, with and without spatially distributed vegetation roughness. Results were analyzed to gain insight into stage-dependent and scale-dependent effects of vegetation on velocities, depths, and flow patterns. At the floodplain filling flow of 597.49 m^3/s, adding spatially distributed vegetation roughness parameters caused 8.0 and 7.4% increases in wetted area and mean depth, respectively, while mean velocity decreased 17.5%. Vegetation has a strong channelization effect on the flow, increasing the difference between mid-channel and bank velocities. It also diverted flow away from densely vegetated areas. On the floodplain, vegetation stands caused high velocity preferential flow paths that were otherwise unaccounted for in the unvegetated model runs. For the river as a whole, as discharge increases, overall roughness increases as well, contrary to popular conception.

Keywords: hydraulic modeling; hydraulic roughness; floodplain hydraulics; river vegetation; river velocity; gravel-bed rivers

1. Introduction

Two-dimensional (2D) hydrodynamic models are emerging as a standard for predicting flood conditions. The preference arises from their ability to more accurately predict complex out-of-bank flow patterns (Bates et al., 1992, 1997; Anderson and Bates, 1994; Bates and Anderson, 1996), overbank depositional patterns (Nicholas and Walling, 1997, 1998; Hardy et al., 2000), and stage-dependent thalweg position relative to one-dimensional (1D) models. These models solve the 2D (depth-averaged) Navier-Stokes equations to predict depth, velocity, and inundation extent for site- and reach-scale floods (Bates et al., 1992; Anderson and Bates, 1994). Finite element models reduce the number of nodes and allow for variable element sizes to resolve details of complex topography or bed roughness (Hardy et al., 1999). Conventionally, hydraulic roughness coefficients are generalized as a constant for all nodes in each delineated cover class (Pasternack, 2011; Straatsma and Huthoff, 2011). The overall goal of this study was to implement a distributed roughness parameterization scheme and then investigate its effects on river hydraulics at three spatial scales ranging from 10^{-1} to 10^{3} channel widths and for a wide range of flows (0.2 to 20 times bankfull discharge).

1.1. Motivation

Floodplain roughness parameterization is a major concern in 2D modeling. Vegetation has a dynamic effect on flow by causing momentum loss or drag that is dependent on vegetation structure. Flow resistance of different plant species has been explored using flume studies (Kouwen and Li, 1980; Kouwen, 1988; Kouwen and Fathi-Moghadam, 2000) and *in situ* analyses (Straatsma, 2009; Sukhodolov and Sukhodolova, 2010). However, obtained equations require detailed, species-specific inputs about vegetation structure unobtainable for large models. Many 2D models do not spatially distribute roughness or use sufficient detail to accurately predict flood hydrodynamics (Marks and Bates, 2000). Roughness values lumped by cover classes are typically empirically estimated or calibrated within an uncertain, acceptable range until results match observations (Bates and Anderson, 1996; Bates et al., 1997). However, this methodology lacks a physical basis. The accuracy value of 2D over 1D modeling stems from its spatially explicit representation of boundary conditions (Brown and Pasternack, 2009; Pasternack and Senter, 2011) and ability to capture 2D flow patterns, both of which should be sensitive to roughness distribution.

1.2. Distributed roughness concepts

Airborne Light Detection and Ranging (LiDAR) can map vegetation presence and canopy height with ~ 4-8 observations per 1 m^2, enabling accurate averaging to resolve 1-m^2 features over large areas (Menenti and Ritchie, 1994; Cobby et al., 2001). Data from LiDAR has yielded spatially distributed roughness maps for 2D modeling (Cobby et al., 2003; Mason et al., 2003; Antonarakis, 2008) by borrowing relationships between vegetation height and hydraulic roughness from flume studies (Kouwen, 1988; Kouwen and Fathi-Moghadam, 2000). Multispectral remote sensing and LiDAR data can be used in tree-segmentation algorithms to classify vegetation based on more detailed parameters such as species, vegetation density, leaf area index, biomass, and basal area (e.g., Antonarakis et al., 2008; Straatsma and Baptist, 2008; Watershed Sciences, 2010). Then a force balance can be applied to determine a roughness coefficient at each node.

A roughness parameterization method using LiDAR data was developed that diverges from traditional approaches. Using equations from atmospheric mixing-layer theory above vegetation canopies (Raupach et al., 1996), Katul (2002) hypothesized that the vertical velocity profile (including the region with roughness elements) above a riverbed follows a hyperbolic tangent distribution with an inflection at the top of the roughness element (Fig. 1). By integrating this velocity profile, an equation was derived for hydraulic roughness as a function of vegetation height and water depth. Casas et al. (2010) used Katul et al.'s (2002) results to demonstrate that spatially distributed, stage-dependent roughness values consistent with accepted literature values could be obtained for 2D models from LiDAR-derived canopy heights and estimated water depths for an ~ 500-m^2 floodplain area. Most importantly, this scheme is easily scalable to vastly larger areas at 1-m resolution, as demonstrated herein. This enables new scientific research on the role of vegetation on river hydraulics.

1.3. Objectives

This study sought to statistically describe and qualitatively explain scale-dependent effects of spatially distributed bank and floodplain vegetation by applying Katul's (2002) methodology to a multimillion node, 2D, finite-volume model that solves the depth-averaged Reynolds equations within an ~ 1-3-m nodal mesh grid for a 28.3-

km river corridor over roughly three orders of magnitude of flow. Specifically, the two objectives of this research were to (i) compare modeled inundation extents, depths, and velocities using stage-dependent, spatially distributed roughness for floodplain vegetation with a constant nodal roughness model excluding vegetation for flows ranging from 0.2 to 20 times bankfull discharge at segment (10^3-10^4 channel widths (W)), reach (10^2-10^3 W), and morphological unit (1-10 W) spatial scales; and (ii) analyze the sensitivity of scale-dependent hydraulic features to the use of spatially distributed roughness values versus a constant roughness scheme. The study presented herein demonstrates that incorporating spatially distributed vegetated roughness has a significant effect on hydrodynamic models by channelizing the thalweg velocities, generating a complex pattern of velocity minima and maxima on the floodplain, and creating backwater depths that increase the wetted area for a given discharge.

2. Study area

The Yuba River is a tributary of the Feather River in north-central California, USA, that drains 3480 km^2 of the western Sierra Nevada range (Fig. 2). Historic hydraulic mining yielded massive alluvial storage in the valley. Englebright Dam, completed in 1940, traps nearly all sediment, promoting a downstream geomorphic recovery that continues today (Carley et al., 2012). The 37.1-km river segment between Englebright Dam and the Feather River confluence is defined as the lower Yuba River (LYR) (Fig. 2), a single-thread channel (~ 20 emergent bars/islands at bankfull) with low sinuosity, high width-to-depth ratio, mean bed slope of 0.185%, mean bed surface sediment size of 97 mm (i.e., small cobble), and slight to no entrenchment. The river corridor is confined in a steep-walled bedrock canyon for the upper 3.1 km, then transitions first into a wider confined valley with some meandering through Timbuctoo Bend, then into a wide, alluvial valley downstream to the mouth. Sediment berms train the active river corridor to isolate it from the ~ 4000 ha Yuba Goldfields. Daguerre Point Dam (DPD) is an 8-m-high irrigation diversion dam 17.8 km upstream of the Feather that creates a slope break and partial sediment barrier. Existing literature with more information about the hydrogeomorphology of the LYR include Pasternack (2008), Moir and Pasternack (2008, 2010), James et al. (2009), Sawyer et al. (2010), White et al. (2010), and Wyrick and Pasternack (2012).

This study investigated 28.3 km of the LYR in the wide, alluvial valley (starting at 39°13'13" N, 121°20'7" W). In addition to assessing segment-averaged effects, the river was segregated into five geomorphic reaches (Fig. 2) and 31 morphological units (MUs) (i.e., subwidth-scale landforms). Seven MUs (i.e., chute, floodplain, lateral bar, point bar, pool, riffle, and run) were used in this study to exemplify the effects of spatially distributed roughness at the MU scale. Full landform descriptions and analyses at segment, reach, and MU scales is available in Wyrick and Pasternack (2012).

Because of insufficient surficial sand and mud in the LYR as well as frequent and aggressive overbank floods, woody vegetation covers 22% of the entire ~ 37.5 km of LYR floodplain (i.e., inundation area for 597.49 m^3/s), with reach coverages in the study domain varying from 16.7% for Marysville to 29.8% for DPD. The Marysville reach has the tallest woody vegetation (average height of 8.6 m) compared to 5.6 m for the DPD reach. Much woody vegetation aligns in patches along current or historic banks. Dense vegetation stands in swales, side channels, and backwaters also exist. The riparian forest is dominated by Fremont cottonwood (*Populus fremontij*), white alder (*Alnus rhombifolia*), and willow (primarily *Salix lasiandra*, *S. hindsiana*, *S. goodingii var. racemosa*, and *S. laevigata*). Herbaceous vegetation is a mix of native and exotic species including rushes (*Junells spp*.), sedges (*Carex spp.*), bull thistle (*Circium vulgare*), mullein (*Verbascum Thapsus*), cocklebur (*Xanthium strunarium var. canadense*), and several exotic grasses (*Bromus spp., Avena spp*.) (Beak Consultants, Inc., 1989).

3. Methods

3.1. Bare earth and canopy digital surface models

All data in the study were collected or generated in English units consistent with regulatory requirements and then converted to SI units for this article, hence the appearance of some unusual values in SI units (e.g., 0.9144 m represents a 3-foot raster cell size). Airborne LiDAR data of bare earth elevation (last returns) and vegetation canopy height (first returns) were collected on 2008 September 21 by Aero-Metric, Inc. (Seattle, WA) during a constant low flow. Overall, terrestrial point spacing and density were 0.427 m and 554 points/100 m^2, respectively. Compared against 8769 road observations, 84.7% of LIDAR points were within 0.06 m, 14.0% were within 0.12 m, and almost all of the rest were within 0.18 m.

Professional bathymetric surveys (± 0.5 feet vertical accuracy) by Environmental Data Solutions (San Rafael, CA) were done during low flows in August and September 2008 as well as during higher flows in March and May 2009 to fill in some unwadable data gaps. Remaining data gaps were filled with real-time kinematic global positioning system (RTK GPS) and total station observations. Combining LiDAR and bathymetric data for the exposed and submerged riverbed, respectively, the overall point spacing and density were 1.28 m and 59.8 points/100 m^2, respectively.

Quality assurance and control procedures were used to produce a digital elevation model (DEM). Data collected using different methods were all compared where they overlapped. For example, 75, 91, and 99% of boat-based water surface elevation (WSE) measurements were within 3, 6, and 15 cm of those from ground-based RTK GPS at the adjacent water's edge, respectively.

Points were visualized as a map in ArcGIS® 9.3.1 (ESRI, Redlands, CA) and further edited on a spatial basis to remove any obvious errors. In narrow backwater channels and along banks that contained obvious interpolation errors, hydro-enforced breaklines and regular breaklines were created to better represent landform features. Additionally, some bathymetric areas that contained very few points because of obstructions and other problematic features were artificially augmented to represent observed channel characteristics. Using the final point cloud, triangulated irregular network (TIN) and raster DEMs were produced following the textbook of Pasternack (2011).

A vegetation canopy height surface model was developed by Watershed Sciences (Portland, OR) and delivered in the form of a 0.9144-m (3-foot) resolution ESRI grid file as documented in Watershed Sciences (2010). Noise points and secondary returns from the vegetation class were excluded by a two-step automated process classifying all first returns ≥ 0.305 m (1 foot, which is two standard deviations of the expected laser noise range) above a localized corrected ground surface as vegetation points. An elevation raster representing the highest LiDAR return classified as vegetation in each cell was created and then filled with values from the bare earth TIN in cells with no LiDAR returns. Finally, ground elevations were subtracted from vegetation elevations to obtain canopy heights, with height < 0.61 m excluded.

3.2. 2D model meshes

The hydrodynamic model used in this study was the U.S. Bureau of Reclamation finite-volume code, SRH-2D (Lai, 2008). The Surface-water Modeling System® (SMS) version 10.1 graphical user interface (Aquaveo, LLC, Provo, UT) was used to produce meshes. Because of the large extent (~ 28.3 km) and meter-scale resolution, the river was split into three domains (Fig. 2). Mesh resolution ranged from 0.9144-m spacing for low flow (in-channel) meshes (28.32-141.58 m^3/s) to 3.05-m spacing for higher flow (channel and overbank) meshes (> 141.58 m^3/s). Digital elevation model elevations were interpolated to mesh points using TIN-based interpolation (Pasternack, 2011). Turbulence closure was achieved using the parabolic, zero equation model, with eddy viscosity varying as a function of depth and shear velocity, modified by an eddy viscosity coefficient set to 0.1 based on local studies and expert experience.

The SRH-2D algorithm requires an upstream flow and a corresponding downstream WSE. In order to capture stage-dependent effects of floodplain vegetation, seven flows were modeled relative to bankfull discharge (Q_{bf}): 28.32 m^3/s (0.2 Q_{bf}), 141.58 m^3/s (1.0 Q_{bf}), 283.17 m^3/s (2.0 Q_{bf}), 597.49 m^3/s (4.2 Q_{bf}), 1194.97 m^3/s (8.4 Q_{bf}), 2389.94 m^3/s (16.8 Q_{bf}), and 3126.18 m^3/s (22.0 Q_{bf}). For the two highest test discharges, water spills out beyond the Feather model domain so analyses requiring that domain were only analyzed up to 1194.97 m^3/s. Geomorphic reach- and MU-scale statistics not reliant on that domain were calculated using all discharges. Downstream WSEs were taken from water-level recorders and surveying observations at model flow boundaries. In the few instances those were unavailable, the WSE predicted by a downstream model at a shared boundary was used to condition the next upstream model.

3.3. Unvegetated gravel/cobble roughness

Only 4.4 and 13.7% of the wetted area included woody vegetation at 28.32 and 141.58 m^3/s, respectively. Therefore, estimation of the unvegetated gravel/cobble surface roughness was established by comparing observed versus modeled WSEs for roughness values of 0.03, 0.035, 0.04, 0.045, and 0.05 at observed low discharges in the range of 14.16 to ~170 m^3/s. Across all flows, the mean absolute deviation was smallest and the histogram of signed deviations was closest to centered on zero for the 0.04 value (Barker, 2011), so this value was adopted to characterize the roughness of all open ground.

3.4. Vegetated roughness derivation

Discrete roughness values were assigned to each node using the approach of Casas et al. (2010). According to the derivation, hydraulic roughness parameterized using Manning's *n* (in SI units) can be approximated for a wide, rectangular, open channel with a sufficiently small streamwise slope by the equation:

$$\frac{U}{u_*} = \frac{h^{1/6}}{n\sqrt{g}} \tag{1}$$

where *U* is depth-averaged velocity, u_* is shear velocity, *h* is water depth, and *g* is the gravitational acceleration constant. To solve Equation (1), an independent equation is needed relating depth-averaged velocity to LiDAR-derived canopy height (*D*). For shallow flow with sufficiently tall woody vegetation, the vertical velocity profile is represented by a hyperbolic tangent distribution with parameters constrained by wind tunnel experiments for diverse vegetation types (Raupach et al., 1996; Katul et al., 1998; Katul and Albertson, 1999; Brunet and Irvine, 2000; Scanlon and Albertson, 2001). When the profile is integrated to obtain depth-averaged velocity and simplified algebraically, the result is given by the equations:

$$\frac{U}{u_*} = C_u f(\xi, \alpha) \tag{2}$$

$$f(\xi, \alpha) = 1 + \alpha \frac{1}{\xi} \ln\left(\frac{\cosh\left(\frac{1}{\alpha} - \frac{1}{\alpha}\xi \right)}{\cosh\left(\frac{1}{\alpha} \right)} \right) \tag{3}$$

$$\xi = \frac{h}{D} \quad (4)$$

where C_u is the similarity constant (empirically estimated as 4.5), and α is the characteristic eddy size coefficient (empirically estimated as 1) (Casas et al., 2010). For $\xi > 7$ and $\xi < 0.2$, the velocity profile fits the log-law for a rough-wall boundary layer, so Equation (5) assumes that $0.2 < \xi < 7$ (Katul et al., 2002; Casas et al., 2010). Thus, any raster cell with ξ outside that range was given an *n* value of 0.04. Combining Equation (1) and Equation (2) yields the final equation:

$$n = \frac{h^{1/6}}{\sqrt{g} C_u f(\xi, \alpha)} \quad (5)$$

Because commercial 2D modeling platforms integrate the logarithmic velocity profile to solve for depth-averaged velocity, using Equation (5) to approximate Manning's *n* is not entirely physically based unless the 2D model takes into account a hyperbolic tangent velocity profile. Future 2D codes could do that. For the purposes of this study, model-predicted velocity using SRH-2D was assumed to be compatible with *n* calculated using Equation (5).

3.5. Roughness map formulation

Because of the stage-dependence of vegetated *n*, each model domain required a unique spatially distributed roughness map for each discharge. Initial *h* estimates came from unvegetated models. These estimates were used to make a TIN and then a 1-m ESRI grid of *h* aligned with the *D* raster. Equation (5) was then implemented in each cell to obtain a 1-m raster for vegetated *n* (Fig. 3). The software SMS and SRH-2D cannot handle such a raster, so discrete cell values for *n* were binned with increments of 0.005 (e.g., 0.0525-0.0575, so that the bin is centered on 0.055). Any vegetated $n < 0.04$ was substituted with 0.04; in other words, if vegetated roughness was insignificant, then substrate roughness was considered the dominant effect.

Additional steps were needed to use the *n* raster in SMS. The *n* raster was converted into spatially distributed polygons with the classified value of *n* as their attribute. These polygons were then interpolated to the finite-volume mesh as element material values using SMS. The SMS interpolation process takes the value of the polygon that intersects the centroid of the finite-volume element to be the roughness value of that element. As a result, some meaningful roughness variation was lost for the 3.05-m meshes. Models were then run with the new spatially distributed roughness using unvegetated solutions as initial conditions.

A vegetated model run produces a different depth and wetted area, so iteration was used until results were stabilized. This process involved using the *h* raster from the first vegetated run in Equation (5) to obtain an improved *n* raster and then running the model again. Each successive run yielded asymptotic convergence (Fig. 4), with only 1-2 iterations commonly necessary.

3.6. 2D model validation

Extensive model validation was performed for unvegetated model simulations for an order of magnitude of flow range (all flows under ~170 m^3/s with ~4-15% of wetted area vegetated). Observations were generally collected away from vegetation. Validation methods and results were detailed by Barker (2011). Herein, only key validation findings are summarized. Mass conservation between specified input flow and computed output flows was within 1%. As an example of WSE performance relative to the river's mean substrate size of ~10 cm, 197 observations at 24.92 m^3/s for a mean signed deviation of -1.8 mm. For unsigned deviations, 27% were within 3.1 cm, 49% of deviations within 7.62 cm, 70% within 15.25 cm, and 94% within 30.5 cm. From cross-sectional surveys yielding 199 observations, predicted versus observed depths yielded a coefficient of determination (r^2) of 0.66, which is on par with what is commonly reported. Using Lagrangian tracking of an RTK GPS on a floating kayak, surface velocity magnitude was measured at 5780 locations, yielding a predicted versus observed r^2 of 0.79, which is significantly higher than commonly reported. Median unsigned velocity magnitude error was 16%, which is less than commonly reported. Also using Lagrangian tracking, velocity direction was tested at those 5780 points, yielding a predicted versus observed r^2 of 0.80. Median direction error was 4%, with 61% of deviations within 5° and 86% of deviations within 10°. Overall, the 2D model used in this study underwent intensive validation testing for feasible flows using a broad suite of validation metrics, and the model met or exceeded all common standards of 2D model performance.

In this study, 2D modeling was done for a range of floods and hazardous hydraulic conditions for which no model validation by direct manual observation was feasible. This is a common problem in floodplain 2D modeling. High cloud coverage precluded the availability of inundated-area imagery. The available sources not influenced by clouds were too coarse for meaningful comparison against model predictions. However, this study presents an explanatory model conceived to investigate physical processes more than a highly validated model for precise prediction of large floods (Van Asselt and Rotmans, 2002; Murray, 2003, 2007). The latter is a standard that no published articles of flood flows have yet met.

4. Data analysis

Model results were analyzed with respect to specific questions (Table 1) based on a scale-dependent approach to characterize the effects of spatially distributed floodplain vegetation on 2D river hydraulics. Each scale represents a different suite of potential effects of vegetation on river processes and societal values, such as flood management, channel change and resilience, and spatial pattern of stage-dependent physical habitat. Mean differences at the MU scale could affect processes such as maintenance of riffle-pool relief or lateral channel migration by bank scour and point bar deposition. For the segment and reach scales, different tests were applied to gain insight into bulk statistical, reach-stratified, and spatially distributed effects of this roughness parameterization scheme. Table 1 indicates which scales were relevant for which questions. The research goals presented in Table 1 were reduced from a larger set (Abu-Aly, 2012) that is too big for journal length limits. The additional tests required to be excluded to reduce article length examined (i) the spatial pattern and statistical distribution of Manning’s *n*, (ii) the statistical significance of the observed differences between model outputs for each roughness scheme, and (iii) the effects of spatially distributed vegetation roughness parameters on at-a-station hydraulic geometry exponents. For full analysis and results, see Abu-Aly (2012).

A common workflow was used to process model outputs to answer scale-dependent questions (Pasternack, 2011). The SRH-2D code produces nodal outputs for water depth as well as velocity magnitude and direction. Model results for the three model domains were combined to yield the segment-scale point data set for each variable for both the constant and spatially distributed roughness schemes at each discharge. Each point data set was used to make a TIN that was then used to produce a 1-m raster. All the rasters were then clipped to each geomorphic reach and each MU to yield data sets for scale-dependent analyses.

4.1. Test 1: depth and velocity effects

For each simulation, the maximum, mean, and standard deviation of velocity and depth for the entire segment-scale model boundary were tabulated using ArcGIS Spatial Analyst. Mean statistics for the constant nodal roughness model (without vegetation roughness parameterization) were subtracted from the mean statistics for the spatially distributed model (with vegetation roughness parameterization) at each spatial scale. A negative value corresponds to a decrease in mean depth or velocity caused by the addition of vegetation roughness, while a positive value corresponds to an increase in mean depth or velocity for the same reason. All deviations were tested for statistical significance ($p < 0.05$) with a *t* test (full methods and results curtailed for brevity; see Abu-Aly, 2012). Absolute (i.e., unsigned) deviations and their percent changes for mean depth and velocity were then calculated for each flow, plotted as a function of discharge, and interpreted for scientific significance, as almost all were statistically significant.

A two-way test was applied to segment-scale results that compared the two roughness parameterizations for their relative bulk hydraulic statistics as a function of discharge, stratifying the river by in-channel versus overbank areas as well as by vegetation versus open ground. The in-channel area was defined by the model-predicted wetted area at 26.33 m^3/s, a low autumnal flow similar to that at which the LiDAR data of vegetation canopy height was taken so that few vegetated raster cells exist within the boundary. The overbank area is the remainder of the model domain. The vegetated area is defined as the boundary of the 1-m resolution raster of Manning's *n*. Absolute mean differences and percent changes in depth and velocity were calculated for in-channel, overbank, and vegetated areas.

A three-way test was also done in which data were stratified and compared by reach (Fig. 2), discharge, and either in-channel versus overbank or vegetated versus open ground. Absolute mean differences and percent changes in depth and velocity were calculated for three-way stratified results.

4.2. Test 2: inundation area effects

To gain insight into the discharge dependence of this increase, the total wetted area (m^2) for both models at the segment scale was calculated and the difference between the two model parameterization schemes was calculated for each flow. Differences were interpreted for scientific significance.

4.3. *Test 3: process effects*

For each flow, a visual inspection of depth and velocity subtraction rasters (i.e., cell-by-cell differencing between the constant nodal roughness model results and the spatially distributed roughness model results) was carried out to find locations with large changes in depth and velocity caused by the addition of vegetation roughness parameters and to determine any relationships between these locations and specific hydraulic processes. Particular attention was paid to how roughness parameterization affects lateral velocity profile and flow patterns around vegetation stands.

5. Results

5.1. *Vegetation roughness statistics*

Segment-scale vegetated Manning's *n* was found to have a bimodal distribution with a range of 0.04 to 0.343, a mean of ~ 0.182 to 0.193 and a mode of ~ 0.202 to 0.228, depending on discharge (Fig. 5). The nature of Equation (5) suggests that the larger ξ is, the smaller the *n* value. Indeed, this is the common assumption of a submergence effect on roughness that is assumed true for unvegetated rivers (e.g., Smart, 1999). Even though the drowning effect of increasing the discharge in the wetted area at a lower flow was present in the results, it was offset by the presence of new, higher roughness in the additional wetted area at the boundary. In the end, the real effect is that the Manning's *n* distribution shifts toward increased mean and maximum roughness with increasing discharge (Fig. 5). This same effect on segment-scale roughness also ought to occur for unvegetated channels wherever wetted area increases with discharge and the banks/floodplain are at least as rough as the bed.

5.2. Test 1: depth and velocity effects

For the range of modeled discharges, the addition of spatially distributed roughness parameters resulted in an almost universal increase in mean depth and decrease in mean velocity. Differences were statistically significant for both variables for all flows at the segment scale. For the two variables in five reaches at seven discharges, only four out of 68 deviations were not statistically significant. For the two variables in seven MUs at seven discharges, only four out of 98 deviations were not statistically significant. The magnitude of these differences increased with discharge. Although differences at each scale followed a similar overall pattern, significant scale-dependent variability in the differences were observed at segment (Fig. 6), reach (Figs. 7-10), and MU scales (Fig. 11).

5.2.1. Segment-scale results

Segment-scale analysis characterized hydraulic effects of spatially distributed vegetation roughness on systemic metrics as a function of discharge. Model results for velocity and depth were highly sensitive to spatially distributed nodal roughness parameters. This sensitivity was shown to increase with discharge, because of an increase in inundated vegetated areas at higher flows. At the segment scale, the addition of spatially distributed vegetation roughness resulted in an overall decrease in mean velocity (Fig. 6A,C), up to an ~ 0.305 m/s reduction at 1194.97 m^3/s. Although the absolute difference in mean velocity increased with discharge for lower flows, the percent change in mean velocity leveled out above roughly 4 Q_{bf} (597.49 m^3/s), approaching 15%, indicating a loss of discharge independence. The in-channel area was found to be the least affected by the addition of vegetation roughness, with a 5% decrease in mean velocity at 1194.97 m^3/s. Larger differences in mean velocity occurred overbank, with over a 20% decrease in mean velocity at flood flows relative to the constant nodal roughness model. The greatest effect of spatially distributed roughness parameters was within the vegetated areas, with mean velocity decreases of ~40% for flows > 283.17 m^3/s.

The corresponding mean depth increased universally across all flows with the addition of vegetation roughness (Fig. 6B,D). The in-channel area experienced the greatest overall increase in mean depth, 0.365 m increase over the constant nodal roughness model. However, because of a smaller mean depth, the overbank area experienced a larger percent increase in mean depth driven by vegetation, with the area 20% deeper than in the constant roughness scheme. Mean depth increase within the vegetated area was the most significant, up to 0.579 m at 1194.97 m^3/s. The percent increase as well as the absolute increase of mean depth showed strong discharge dependence.

5.2.2. Reach-scale results

Reach-scale analysis of model results accounted for systematic spatial variability in sediment transport capacity and sediment supply that is controlled by valley wall undulations, major slope breaks, base level impacts of dams, and tributary junctions. Reach-scale analyses revealed variability in the effects of vegetation roughness parameters based on individual reach characteristics, but the magnitude of the differences in model results and trends associated with discharge remained similar to segment-scale differences. Mean velocity decreased ~0.305 m/s at 1194.97 m^3/s for most reaches. With the upper and middle reaches of the LYR (i.e., Parks Bar, Dry Creek, and DPD) successfully modeled up to 3126.18 m^3/s, the reach-scale results showed an inflection point in the mean velocity difference and the mean depth difference (Fig. 7A,C) that was otherwise unaccounted for in segment-scale results constrained to 1194.97 m^3/s. Mean velocity changes continued to grow with discharge up to 0.45 to 0.60 m/s at 3126.18 m^3/s. Mean depth increases up to 0.762 m over the constant nodal roughness model were observed at Dry Creek and DPD (Fig. 7B,D). Percent change in mean velocity and mean depth seem to level out after 597.49 m^3/s, with a slightly increasing trend in the reaches where 2389.94 m^3/s and 3126.18 m^3/s were modeled. Flows smaller than Q_{bf} showed changes in depth and velocity of < 5%, consistent with the lower percent coverage of vegetation. Vegetation roughness appeared to have the greatest effect on flows > 2 Q_{bf}.

Flow in the channel showed a much smaller decrease in mean velocity than that flowing beyond the channel (Fig. 7A,C), but the addition of spatially distributed vegetation roughness still had a noticeable effect, decreasing the mean velocity there by 0.15 to 0.25 m/s at 1194.97 m^3/s in all but one reach. The Dry Creek reach, an anastomosing section bounded upstream by a tributary junction, actually experienced an increase in mean velocity in the primary channel at 283.17 and 597.49 m^3/s (Fig. 8A,C). Mean velocity changes in this reach at the two highest flows were noticeably smaller than the other reaches. Mean depth in the main channel increases ubiquitously at all flows (Fig. 7B,D). At the highest flows, mean depth increases from 0.45 to 0.91 m over a model with constant nodal roughness. Above 1194.97 m^3/s, percent changes in depth and velocity leveled out, showing that differences between the two models were scaling with discharge.

Changes in overbank hydraulics at the reach scale were greater than those in the channel, as the overbank area is much larger, shallower, and more vegetated than the main channel (Fig. 9). Mean velocity decreases were observed of 0.45 to 0.61 m/s at higher flows. Mean depth increases were observed from 0.45 to 0.91 m. Although these absolute differences were similar in magnitude to reach statistics, overbank areas had lower mean velocity and depth than the channel. This resulted in generally higher percent changes in mean velocity and depth in the floodplain. Mean velocity showed a 20-25% decrease at the highest flow for most reaches. The DPD reach experienced a 35% decrease in mean velocity at 3126.18 m^3/s. The DPD reach is unique in the LYR because (as a result of the pattern of historical aggregate extraction) it contains a parallel floodway separated by a long, isolated training berm, including an inset channel that is activated between 283.17 and 424.75 m^3/s. This could account for the large differences in velocity at higher flows, where the percent of flow contained in each branch of the channel becomes shared nearly equally at the highest discharges. Mean depth percent differences in the overbank area varied significantly depending on the reach. Above 1194.97 m^3/s, Parks Bar reach held a steady ~15% increase in mean depth over the bare model. In this same range, Dry Creek and DPD showed a 25-30% increase in mean depth.

Changes within vegetated areas were the most significant (Fig. 10). Mean velocity decreases of 0.75 to 0.88 m/s and mean depth increases of 0.74 to 1.11 m were observed throughout all the reaches at the highest flows when compared with the model with an *n* of 0.04. Interestingly, mean velocity percent changes for all reaches above 283.17 m^3/s (Dry Creek above 1194.97 m^3/s) were clustered in a tight band between 35 and 40%. The 35 to 40% change takes into account a wide range of roughness coefficients, spatially distributed according to vegetation presence throughout each reach. This implies that above a certain flow threshold, the localized effects on mean velocity of changing the roughness coefficient of an element are a constant function of discharge. Mean depth percent increase in the vegetated areas was much more sensitive to reach characteristics. Adding vegetation roughness to the bare model caused a 15-30% increase in mean depth above 1194.97 m^3/s, depending on the reach. Again, Parks Bar was the least affected within ~ 15% increase in mean depth, while DPD and Dry Creek exhibited changes in mean depth of ~ 30% above 1194.97 m^3/s.

5.2.3. MU-scale results

Results at the MU scale showed the effects of spatially distributed roughness parameters on hydraulics over discrete landforms. Mean depth and mean velocity differences were shown to increase with discharge. However, because of relatively different depths and velocities associated with each landform, percent changes were shown to vary by unit (Fig. 11). In-channel bed units were least affected by spatially distributed vegetation roughness parameters, with mean velocity changes of < 3% across all flows. Mean depth changes were slightly more noticeable, but still < 11% in riffles and pools across all flows. Nevertheless, these MUs were not immune to roughness changes off-channel.

Bank and floodway units exhibited much greater sensitivity to spatially distributed roughness, because of the large presence and influence of vegetation on those landforms. Floodplains experienced a mean velocity decrease of 0.036 m/s at 283.17 m^3/s, a 9.5% decrease, up to a mean velocity decrease of 0.256 m/s at 1194.97 m^3/s, a 20% decrease. At 1194.97 m^3/s, the floodplain unit experienced a 32% increase in mean depth. Lateral bars experienced an ~ 20% decrease in mean velocity at all flows above 28.32 m^3/s. Point bars were also largely affected above 28.32 m^3/s with mean velocity decreasing 13.5 to 16.0% in this unit. While velocities on the floodplain experienced a mean decrease, instances of flow acceleration through vegetation patches in flood runners (i.e., ephemeral channels on the floodplain) occurred with an increase in the maximum velocity by 0.116 m/s, even though the MU-averaged velocity decreased.

5.3. Test 2: inundation area effects

Differences in model-predicted inundation extents (Table 2; Fig. 12) showed that mean depth and total wetted area increased across all flows when spatially distributed vegetation roughness was used. The absolute difference and percent change in inundated area increased with discharge up to 597.49 m^3/s. At this flow, the addition of vegetated roughness increased the total wetted area of the flow by 616,224 m^2, an 11.7% increase. A slight drop off in total wetted area increase occurred at the highest flow, 1194.97 m^3/s, with only a 7.3% increase. Inundation extent was not as sensitive to the roughness parameterization scheme as mean depth and mean velocity; however, an 11.7% increase in the total wetted area can represent a significant difference for flood risk managers.

5.4. Test 3: process effects

The addition of spatially distributed vegetated roughness had a significant effect on the predicted occurrence and distribution of specific hydraulic processes. Floodplain hydraulic complexity and cross-channel parabolic velocity profile are two key processes impacted by choice of roughness scheme. At ~ 8 Q_{bf}, model-predicted velocities with vegetated roughness showed a significant increase in overbank flow complexity when compared to a model of the same flow with a constant nodal roughness (Fig. 13). A cross section of the lateral velocity profile shows significantly more variability in velocity, with clearly defined concentrations of faster flow along unvegetated pathways and significantly slower flow within the vegetation itself (Fig. 14). Differences in the velocity profile of ~ 1 m/s were observed within the vegetated areas. Mid-channel flow velocities were also shown to be sensitive to vegetation roughness parameters, even in the thalweg far from vegetation.

Changes in velocity in the spatially distributed roughness model at Q_{bf} were lower than at higher flows (Fig. 15) but still showed significant spatial patterns. Velocity decreases of 0.5 m/s occurred within vegetated areas, while slight increases in mid-channel velocities occurred at the riffle cross section (Fig. 16). This comparison shows that bank-lining vegetation acts as a proxy for bank roughness by channelizing thalweg velocities, focusing higher velocities away from the bank slopes. However, much of the main channel is not significantly affected by vegetation roughness at this flow, except in channel constrictions and riffle crests where bank-lining vegetation causes an increase in velocity.

6. Discussion

6.1. Composition of roughness from vegetation

Lower Yuba River substrates include heterogeneous gravel/cobble, but a key finding of this study was that the range of roughness associated with substrate is significantly smaller than that associated with the range of vegetation. Manning's *n* values for substrate patches with different mixtures of gravel and cobble could range from ~ 0.03 to 0.05, and considering boulders and bedrock in some locations perhaps up to ~ 0.06 to 0.075. Some studies have found that bed roughness decreases with increasing stage because of relative roughness, but where the incrementally new wetted areas add more roughness to the bed or emergent in-channel features become submerged that effect is not evident. For example, in the site-scale 2D model studies of the LYR by Fulton (2008) and Sawyer et al. (2010), unvegetated riverbed roughness was calibrated using observed WSE for a wide range of discharges above and below Q_{bf}. No systematic variation in bed roughness was found in those studies, with stage-dependent fluctuations limited to a narrow range of ~0.03-0.05.

In contrast, this study found that Manning's *n* values for woody vegetation patches ranged from 0.04 to 0.343, which is much wider than observed for unvegetated substrate. Sawyer et al. (2010) conducted a detailed allometric analysis of the vegetated riverbank along a pool-riffle-run complex upstream of the segment in this study on the LYR to carefully estimate a single roughness value of 0.057. That value is within the range observed in this study, but this study found that patches of that size include an order-of-magnitude range of values and that range is dynamic over an order-of-magnitude when flow changes over roughly three orders of magnitude. This qualitative sensitivity analysis leads to the conclusion that model accuracy benefit more from investing in spatially distributed woody vegetation roughness parameterization than spatially distributed substrate roughness parameterization in vegetated areas. Further, a simpler, spatially distributed approach is more important to 2D modeling than a detailed analysis of local vegetated structure, such as may be done using terrestrial LiDAR, allometric characterization, or other plant-scale manual measurements.

However, metrics evaluated across such a large number of elements begin to call into question the roughness parameterization method itself and whether or not it is indeed physically based. Manning's roughness in 2D models would ideally be representative of the structural characteristics of the ground cover and the momentum loss associated with it. A degree of unquantified uncertainty in 2D modeling already exists and roughness parameterization using calibration techniques turns the Manning's roughness coefficient into a sink of that uncertainty. The roughness parameterization method proposed by Casas et al. (2010) has merit in the fact that the two input variables are physically based and can be estimated with a large degree of certainty. But, for multimillion element models across an ~ 40-km-long river, similar results could perhaps be obtained with any reasonable woody vegetation roughness parameterization method such as classifying the floodplain and main channel only, or using ostensibly uniform roughness values to account for all of the vegetated areas, or any other method in the current literature. However, such alternate methods tend to be highly subjective and legally disputable compared to the objective algorithm used in this study. Without unfeasibly detailed validation data sets to compare with, the accuracy of roughness parameterization methods will always come into question. Even though the exact calculated values of each nodal roughness coefficient can come under scrutiny, riparian vegetation undeniably causes a varying degree of momentum loss on the flow, as momentum is dependent on the height and density of ground cover. With remote sensing techniques to map the spatial distribution and structural characteristics of vegetation becoming easily obtainable and widely implemented at very large scales, the next generation of 2D models will have to consider, in some sense, the significant effects that floodplain vegetation can have on model outputs.

6.2. Coherent differences

The differences between the two roughness schemes for mean depth and mean velocity were shown to be statistically significant and highly ordered for a wide range of flows. Differences at the segment scale were shown to be significant at all modeled flow rates. Differences at the reach scale were shown to be significant at Q_{bf} and above. Differences at the MU scale were MU-dependent; those with little to no vegetation had less significant deviations than those containing it. Overbank units such as floodplain show much greater sensitivity at flows above Q_{bf} than in-channel units such as riffles and pools. These results suggest that the usefulness of a high resolution, spatial-distributed, vegetation roughness parameterization scheme is limited by the size of the inundated vegetated area. Modeling applications that focus on aquatic microhabitat (i.e., ~ 1-m point scale) in lightly vegetated gravel-bed streams do not need to apply a spatially distributed roughness scheme in order to achieve what would end up as statistically indistinguishable results. However, spatially distributed roughness parameters have a large impact on reach- and segment-scale, multimillion element, hydrodynamic models that include diverse vegetated settings and important floodplain hydraulics questions.

6.3. Stage-dependent river hydraulics

The effects of spatially distributed vegetation roughness increase with discharge for mean depth and velocity across all scales and was ubiquitous in the river above Q_{bf}. Segment- and reach-scale assessments showed that the largest differences between the two roughness schemes occurred overbank within vegetated areas. Percent changes in mean velocity level out above approximately two times Q_{bf}, but absolute differences in mean velocity and depth continue to grow with discharge. The MU-scale results show that the effect of vegetation is greatest in bar and overbank units (where wetted area increases are focused) and that mean velocity and depth differences between the two roughness parameterization schemes increase with discharge in these units. Mid-channel units such as riffles and pools were affected, but less so, because they were not receiving additional local roughness, just experiencing the distal effects of roughness increases elsewhere.

The addition of spatially distributed roughness significantly changed predicted hydraulics. Mean depth increases effectively increased the inundation extents for each flow and raised model-predicted WSEs. Likewise the spatially distributed roughness scheme resulted in significant changes to the lateral velocity profile and decreased mean velocity. Overbank areas experienced significant changes in predicted velocity patterns with complex interactions between flow and vegetation.

For reach- and segment-scale 2D models, a significant difference exists between using a spatially distributed vegetated roughness scheme versus a constant roughness scheme, especially at flows above Q_{bf}. Meter to decimeter resolution hydrodynamic models concerned with flood flows would almost certainly have to apply some sort of spatially distributed roughness parameterization scheme in order to accurately capture overbank flow patterns. While the accuracy of the exact roughness values applied to each node can come under scrutiny depending on the method, high resolution models at all scales clearly are sensitive to small changes in nodal roughness.

6.4. Flood inundation

The addition of spatially distributed roughness parameters to the 2D model increased mean depth universally across all flows, causing a significant increase in area of inundation. The magnitude of this difference varied with discharge, dependent on channel geometry and vegetation patterns. Rivers with broad, vegetated active floodplains or braidplains would experience a larger increase in model-predicted inundation extent than rivers with steep valley walls. This particular metric has a significant effect on flood risk modeling where accurate prediction of flood boundaries can mean the difference between flood waters being contained within or overtopping bounding levees. Inundation extent also affects physical habitat modeling where shallow depths in vegetated channel margins account for juvenile salmonid rearing habitat.

6.5. Key hydraulic processes

Observation of the local effects of vegetation roughness parameters on hydraulics illustrated the spatial structure of the statistical changes characterized in the previous tests. Spatially distributed vegetation roughness parameters have a significant effect on in-channel and overbank hydraulic patterns. Complex interactions between modeled depths, velocities, and vegetation are revealed that would seem to be physically based. This has broad-reaching implications for the design and application of hydrodynamic models across a range of scientific disciplines. Several fish habitat metrics (e.g., extent of shallow water, habitat heterogeneity in floodplain refugia, and covered habitat conditions along banks) rely on accurately modeled depths and velocities at the microhabitat scale. Predicting erosional patterns based on modeled shear stresses requires accurate representation of the 2D velocity field. River rehabilitation projects may rely on MU- and reach-scale models of overbank flow patterns to characterize high flow channels that can harbor riparian vegetation and fish-rearing habitat. Flood risk management relies on accurate inundation extent maps taken from hydraulic model results at the segment scale. The results presented in this study have shown that parameterization of floodplain vegetation roughness greatly affected predicted model output at all scales investigated.

7. Conclusions

Spatially distributed roughness parameters in 2D models were found to yield a significant effect on 2D hydraulic model results. The extent of the sensitivity of model results is both stage- and scale-dependent. With the spatially distributed roughness model, mean water depth increased up to 0.8 m (25%) and mean depth-averaged velocity decreased by up to 0.6 m/s (30%) at the maximum modeled discharge of 3126.18 m^3/s (22 Q_{bf}) when compared to the constant roughness model. At 141.58 m^3/s (Q_{bf}), these differences were on the order of a 5% decrease in mean depth-averaged velocity and a 1% increase in mean water depth. These results show the range and magnitude of differences that roughness parameters can have on 2D model output and reflect the importance of accurately mapping, characterizing, and accounting for riparian vegetation in 2D hydraulic river models. Remote sensing techniques to map the spatial distribution and structural characteristics of vegetation are now easily obtainable and widely implemented at very large scales. As the spatial discretization of hydraulic models gets smaller with increases in computing power, model results will represent ever smaller spatial scales and in more detail than current 2D models. Vegetation presence mapping is already at the level of spatial resolution of digital elevation models, and in the efforts to achieve predictive hydrodynamic modeling, roughness parameterization must take on this same level of detail.

8. Acknowledgements

Financial support for this work was provided by Pacific Gas & Electric Company, the U.S. Fish and Wildlife Service Anadromous Fish Restoration Program (Agreement #113323J011), Yuba County Water Agency, and the Yuba Accord River Management Team Award #201016094. We acknowledge Professors Tim Ginn and Fabian Bombardelli (UC Davis Civil & Environmental Engineering) for helpful reviews of the manuscript prior to submission as well as anonymous reviewers who guided revision and editor Dick Marston for a thorough editor's markup.

9. References

Abu-Aly, T.R., 2012. Effects of LiDAR-derived, spatially-distributed vegetation roughness on 2D hydraulics in a gravel-cobble river at flows of 0.2 to 20 times bankfull. M.S. Thesis, University of California at Davis, Davis, CA.

Anderson, M.G. Bates, P.D., 1994. Evaluating data constraints on two dimensional finite element models of floodplain flow. Catena 22(1), 1-15.

Antonarakis, A.S., 2008. The potential of LiDAR in recovering physical data on floodplain vegetation to parameterise flow resistance. Ph.D. dissertation, Cambridge University, UK.

Antonarakis, A.S., Richards, K., Brasington, J., Muller, E., Bithell, M., 2008. The use of Airborne lidar to retrieve vegetative fluid resistance terms for rigid stems. In: Remote Characterization of Vegetation Structure, Special Issue Journal of Geographical Research-Biogeosciences 113, G02S07. doi:10.1029/2007JG000543.

Barker, J.R. 2011. Rapid, abundant velocity observation to validate million-element 2D hydrodynamic models. M.S. Thesis, University of California at Davis, Davis, CA.

Bates, P.D., Anderson, M.G., 1996. A preliminary investigation into the impact of initial conditions on flood inundation predictions using a time/space distributed sensitivity analysis. Catena 26(1-2), 115-134.

Bates, P.D., Anderson, M.G., Baird, L., Walling, D.E. Simm, D., 1992. Modeling floodplain flows using a two-dimensional finite element model. Earth Surface Processes and Landforms 17(6), 575-588.

Bates, P.D., Anderson, M.G., Hervouet, J.M., Hawkes, J.C., 1997. Investigating the behaviour of two-dimensional finite element models of compound channel flow. Earth Surface Processes and Landforms 22(1), 3-17.

Beak Consultants, Inc., 1989. Yuba River fisheries investigations, 1986-88. Summary Report of Technical Studies on the Lower Yuba River, California. Sacramento, CA.

Brown, R.A., Pasternack, G.B., 2009. Comparison of methods for analyzing salmon habitat rehabilitation designs for regulated rivers. River Research and Applications 25, 745-772.

Brunet, Y., Irvine, M.R., 2000. The control of coherent eddies in vegetation canopies: streamwise structure spacing, canopy shear scale and atmospheric stability. Boundary Layer Meteorology 94, 139-163.

Carley, J.K., Pasternack, G.B., Wyrick, J.R., Barker, J.R., Bratovich, P.M., Massa, D.A., Reedy, G.D., Johnson, T.R., 2012. Significant decadal channel change 58-67 years post-dam accounting for uncertainty in topographic change detection between contour maps and point cloud models. Geomorphology, doi:10.1016/j.geomorph.2012.08.001.

Casas, A., Lane, S.N., Yu, D., Benito, G., 2010. A method for parameterising roughness and topographic sub-grid scale effects in hydraulic modelling from LiDAR data. Hydrology and Earth System Sciences 14, 1567-1579, doi:10.5194/hess-14-1567-2010.

Cobby, D.M., Mason, D.C., Davenport, I.J., 2001. Image processing of airborne scanning laser altimetry data for improved river flood modelling. International Society for Photogrammetry and Remote Sensing Journal of Photogrammetry and Remote Sensing 56(2), 121-138.

Cobby, D.M., Mason, D.C., Horritt, M.S., Bates, P.D., 2003. Two-dimensional hydraulic flood modelling using a finite-element mesh decomposed according to vegetation and topographic features derived from airborne scanning laser altimetry. Hydrological Processes 17(10), 1979-2000.

Fulton, A.A., 2008. Gravel for salmon in bedrock channels: elucidating mitigation efficacy through site characterization, 2D-modeling, and comparison along the Yuba River, CA. M.S. Thesis, University of California at Davis, Davis, CA.

Hardy, R.J., Bates, P.D., Anderson, M.G., 1999. The importance of spatial resolution in hydraulic models for floodplain environments. Journal of Hydrology 216(1-2), 124-136.

Hardy, R.J., Bates, P.D., Anderson, M.G., 2000. Modelling suspended sediment deposition on a fluvial floodplain using a two-dimensional dynamic finite element model. Journal of Hydrology 229(3-4), 202-218.

James, L.A., Singer, M.B., Ghoshal, S., Megison, M., 2009. Historical channel changes in the lower Yuba and Feather Rivers, California: long-term effects of contrasting river-management strategies. In: James, L.A., Rathburn, S.L., Whittecar, G.R. (Eds.), Management and Restoration of Fluvial Systems with Broad Historical Changes and Human Impacts. Geological Society of America Special Paper 451, Boulder, CO, pp. 57-81; http://dx.doi.org/10.1130/2008.2451(04).

Katul, G.G., Albertson, J.D., 1999. Low dimensional turbulent transport mechanics near the forest-atmosphere interface. In: Bayesian Inference in Wavelet-based Models. Lecture Notes in Statistics 141, Springer-Verlag, New York, pp. 361-380.

Katul, G.G., Geron, C.D., Hsieh, C.I., Vidakovic, B., Guenther, A.B., 1998. Active turbulence and scalar transport near the land-atmosphere interface. Journal of Applied Meteorology 37, 1533-1546.

Katul, G.G., Wiberg, P., Albertson, J., Hornberger, G., 2002. A mixing layer theory for flow resistance in shallow streams. Water Resources Research 38(11), 1250.

Kouwen, N., 1988. Field estimation of the biomechanical properties of grass. Journal of Hydraulic Research 26(5), 559-568.

Kouwen, N., Fathi-Moghadam, M., 2000. Friction factors for coniferous trees along rivers. Journal of Hydraulic Engineering-ASCE 126(10), 732-740.

Kouwen, N., Li, R.M., 1980. Biomechanics of vegetative channel linings. Journal of the Hydraulics Division-ASCE 106(6), 1085-1106.

Lai, Y.G., 2008. SRH-2D Version 2: Theory and User's Manual. U.S. Department of the Interior, Bureau of Reclamation, Technical Service Center, Denver, CO.

Marks, K., Bates, P., 2000. Integration of high-resolution topographic data with floodplain flow models. Hydrological Processes 14(11-12), 2109-2122.

Mason, D.C., Cobby, D.M., Horritt, M.S., Bates, P.D., 2003. Floodplain friction parameterization in two-dimensional river flood models using vegetation heights derived from airborne scanning laser altimetry. Hydrological Processes 17(9), 1711-1732.

Menenti, M., Ritchie, J.C., 1994. Estimation of effective aerodynamic roughness of walnut gulch watershed with laser altimeter measurements. Water Resources Research 30(5), 1329-1337.

Moir, H.J., Pasternack, G.B., 2008. Relationships between mesoscale morphological units, stream hydraulics and Chinook salmon (*Oncorhynchus tshawytscha*) spawning habitat on the Lower Yuba River, California. Geomorphology 100, 527-548.

Moir, H.J., Pasternack, G.B. 2010. Substrate requirements of spawning Chinook salmon (*Oncorhynchus tshawytscha*) are dependent on local channel hydraulics. River Research and Applications 26, 456-468.

Murray, A.B., 2003. Contrasting the goals, strategies, and predictions associated with simplified numerical models and detailed simulations. In: Wilcock, P.R., Iverson, R.M. (Eds.), Prediction in Geomorphology. American Geophysical Union, Washington, DC, doi: 10.1029/135GM11.

Murray AB., 2007. Reducing model complexity for explanation and prediction. Geomorphology 90 (3-4), 178-191.

Nicholas, A.P., Walling, D.E., 1997. Modelling flood hydraulics and overbank deposition on river floodplains. Earth Surface Processes and Landforms 22(1), 59-77.

Nicholas, A. P., Walling, D. E., 1998. Numerical modelling of floodplain hydraulics and suspended sediment transport and deposition. Hydrological Processes 12, 1339-1355.

Pasternack, G.B., 2008. SHIRA-Based River analysis and field-based manipulative sediment transport experiments to balance habitat and geomorphic goals on the lower Yuba River. University of California at Davis Technical Report, Davis, CA.

Pasternack, G. B., 2011. 2D Modeling and Ecohydraulic Analysis. Createspace, Seattle, WA.

Pasternack, G. B., Senter, A.E., 2011. 21st Century instream flow assessment framework for mountain streams. California Energy Commission, Public Interest Energy Research, CEC-500-2013-059, Sacramento, CA.

Raupach, M.R., Finnigan, J.J., Brunet, Y., 1996. Coherent eddies and turbulence in vegetation canopies: the mixing-layer analogy. Boundary-Layer Meteorology 78(3-4), 351-382.

Sawyer, A.M., Pasternack, G.B., Moir, H.J., Fulton, A.A., 2010. Riffle-pool maintenance and flow convergence routing confirmed on a large gravel bed river. Geomorphology 114, 143-160.

Scanlon, T.M., Albertson, J.D., 2001. Turbulent transport of carbon dioxide and water vapor within a vegetation canopy during unstable conditions: identification of episodes using wavelet analysis. Journal of Geophysical Research 106, 7251-7262.

Smart, G.M., 1999. Turbulent velocity profiles and boundary shear in gravel bed rivers. Journal of Hydraulic Engineering 125, 106–116.

Straatsma, M., 2009. 3D float tracking: in situ floodplain roughness estimation. Hydrological Processes 23(2), 201-212.

Straatsma, M.W., Baptist, M., 2008. Floodplain roughness parameterization using airborne laser scanning and spectral remote sensing. Remote Sensing of Environment 112(3), 1062-1080.

Straatsma, M., Huthoff, F., 2011. Uncertainty in 2D hydrodynamic models from errors in roughness parameterization based on aerial images. Physics and Chemistry of the Earth, Parts A/B/C 36(7-8), 324-334.

Sukhodolov, A.N., Sukhodolova, T.A., 2010. Case study: effect of submerged aquatic plants on turbulence structure in a lowland river. Journal of Hydraulic Engineering-ASCE 136(7), 434-446.

Van Asselt, M.B.A., Rotmans, J. 2002. Uncertainty in integrated assessment modelling—from positivism to pluralism. Climactic Change 54, 75-105.

Watershed Sciences, 2010. Riparian Mapping And Classification Delivery 1: Existing LiDAR Reclassification- Revision 1.0, Lower Yuba River, CA. Watershed Sciences, Corvallis, OR.

White, J.Q., Pasternack, G.B., Moir, H.J., 2010. Valley width variation influences riffle-pool location and persistence on a rapidly incising gravel-bed river. Geomorphology 121, 206-221.

Wyrick, J.R., Pasternack, G.B., 2012. Landforms of the Lower Yuba River. Prepared for The Lower Yuba River Accord Planning Team. University of California at Davis, Davis, CA.

Figure Captions:

Fig. 1. Schematic of the mixing layer in shallow streams.

Fig. 2. Lower Yuba River study area, including the location of the watershed in the United States and California, 2D model reach domains, and geomorphic reaches.

Fig. 3. Sample of one Manning's n raster (1-m resolution; 3126.18 m^3/s).

Fig. 4. Convergence of WSE through model iterations with refined water depth inputs to Equation (5) (Hammon reach at 597.49 m^3/s).

Fig. 5. Manning's n histograms for () 28.32 m^3/s, (B) 141.58 m^3/s, (C) 283.17 m^3/s, (D) 597.49 m^3/s, and (E) 1194.97 m^3/s.

Fig. 6. Mean differences for velocity (A) and depth (B); mean percent difference for velocity (C) and depth (D) for the segment scale.

Fig. 7. Mean differences for velocity (A) and depth (B); mean percent difference for velocity (C) and depth (D) stratified by reach and using the entire wetted area at each flow.

Fig. 8. Mean differences for velocity (A) and depth (B); mean percent difference for velocity (C) and depth (D) stratified by reach but only within the channel.

Fig. 9. Mean differences for velocity (A) and depth (B); mean percent difference for velocity (C) and depth (D) stratified by reach, but only out of the channel.

Fig. 10. Mean differences for velocity (A) and depth (B); mean percent difference for velocity (C) and depth (D) stratified by reach and within vegetated areas.

Fig. 11. Mean differences for velocity (A) and depth (B); and mean percent difference for velocity (C) and depth (D) stratified by morphological unit.

Fig. 12. Wetted area comparison between the spatially distributed vegetated roughness model and the model with constant unvegetated roughness.

Fig. 13. Overbank velocity differences between the two roughness schemes at 1194.97 m^3/s.

Fig. 14. Lateral velocity profile cross section at 1194.97 m^3/s.

Fig. 15. Mid-channel velocity differences between the two roughness schemes at Q_{bf}.

Fig. 16. Lateral velocity profile cross section at Q_{bf}.

Table *1*

Research questions and testing approach

Research goals	Tests applied to evaluate questions[a]
Goal 1: Characterize stage-dependent role of vegetation-induced roughness on river hydraulics.	
1a. What are the statistical differences at each scale between roughness schemes with respect to mean velocity and depth as a function of discharge?	1a. Plot and describe the differences in mean velocity and mean depth versus discharge for each scale. Test statistical significance of differences using *t* test.
1b. Are the most significant effects localized in any specific river-corridor zone at segment and reach scales?	1b. Stratify model results into specific river-corridor zones for comparison, such as channel versus overbank area and unvegetated versus vegetated area.
Goal 2: Characterize the role of vegetation-induced roughness on flood inundation.	
2. How does the addition of spatially distributed roughness affect model predicted inundation extent?	2. Calculate the wetted area for both the uniform roughness model and the spatially distributed roughness model in ArcGIS and compare for each flow (segment scale only).
Goal 3: Analyze response of hydraulic processes to spatial patterns in vegetation-induced roughness.	
3. What are the effects of spatially distributed roughness parameters on specific hydraulic processes, such as in channel lateral velocity profile and overbank flooding?	3. Visual inspection of the spatial distribution of model-predicted velocity and depth difference at individual sites that illustrate the process differences depending on the roughness scheme.

[a]Test applies to all three spatial scales unless otherwise indicated.

Table *2*

Model predicted wetted area and inundated vegetated area

Discharge (m^3/s)	Bankfull factor	Model-predicted wetted area (m^2)		Area increase	Increase (%)	Inundated vegetated area (m^2)	Total wetted area (%)
		With constant nodal roughness	With spatially distributed roughness				
28.32	0.20	1,700,125	1,702,960	2,835	0.17%	14,641	0.86%
141.58	1.00	2,655,223	2,716,310	61,086	2.30%	150,281	5.53%
283.17	2.00	3,415,892	3,759,209	343,316	10.05%	321,106	8.54%
597.49	4.20	5,268,466	5,884,690	616,224	11.70%	906,561	15.41%
1194.97	8.40	7,007,945	7,521,049	513,104	7.32%	1,493,975	19.86%

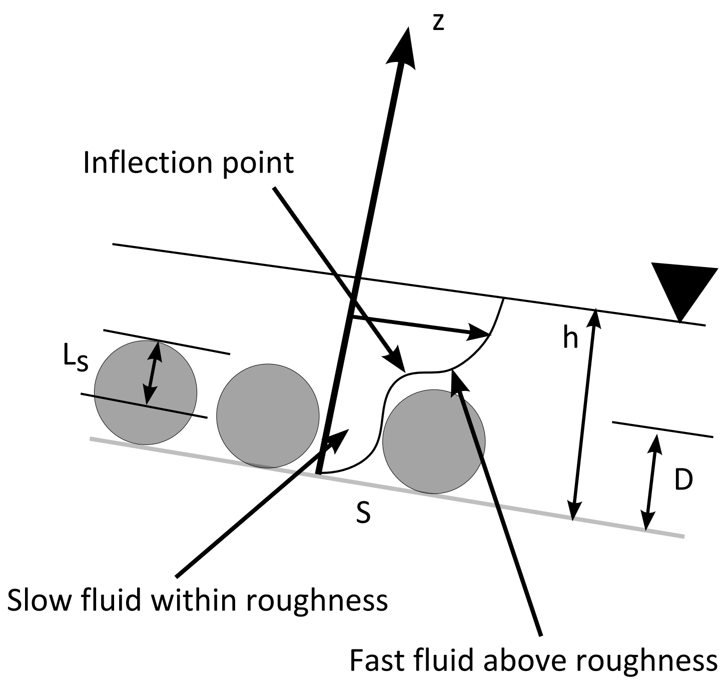

Modified after Casas et al. (2010)

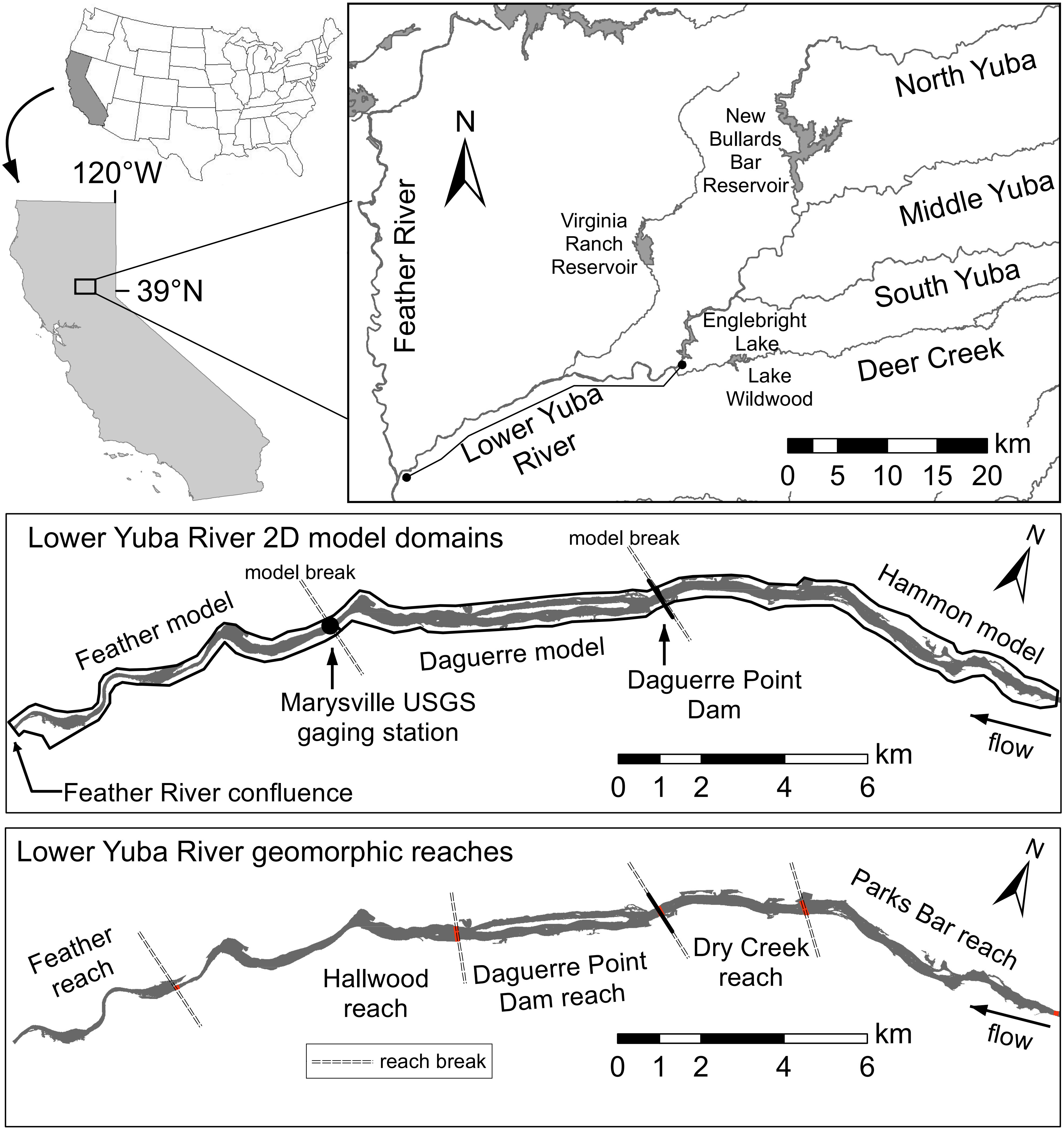
120°W
39°N
N
Feather River
Virginia Ranch Reservoir
New Bullards Bar Reservoir
North Yuba
Middle Yuba
South Yuba
Englebright Lake
Deer Creek
Lake Wildwood
Lower Yuba River
km
0 5 10 15 20
Lower Yuba River 2D model domains
model break
model break
N
Feather model
Daguerre model
Hammon model
Marysville USGS gaging station
Daguerre Point Dam
flow
Feather River confluence
km
0 1 2 4 6
Lower Yuba River geomorphic reaches
N
Feather reach
Hallwood reach
Daguerre Point Dam reach
Dry Creek reach
Parks Bar reach
flow
reach break
km
0 1 2 4 6

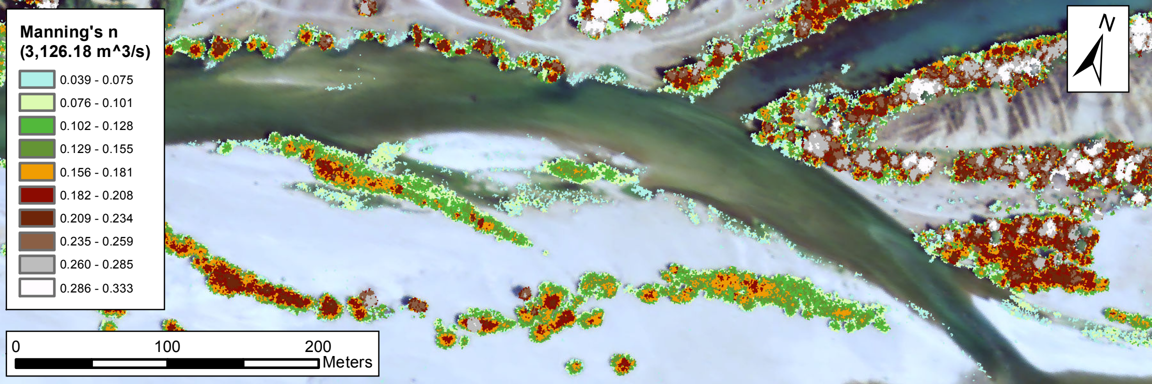
Manning's n
(3,126.18 m^3/s)
0.039 - 0.075
0.076 - 0.101
0.102 - 0.128
0.129 - 0.155
0.156 - 0.181
0.182 - 0.208
0.209 - 0.234
0.235 - 0.259
0.260 - 0.285
0.286 - 0.333
0
100
200
Meters
N

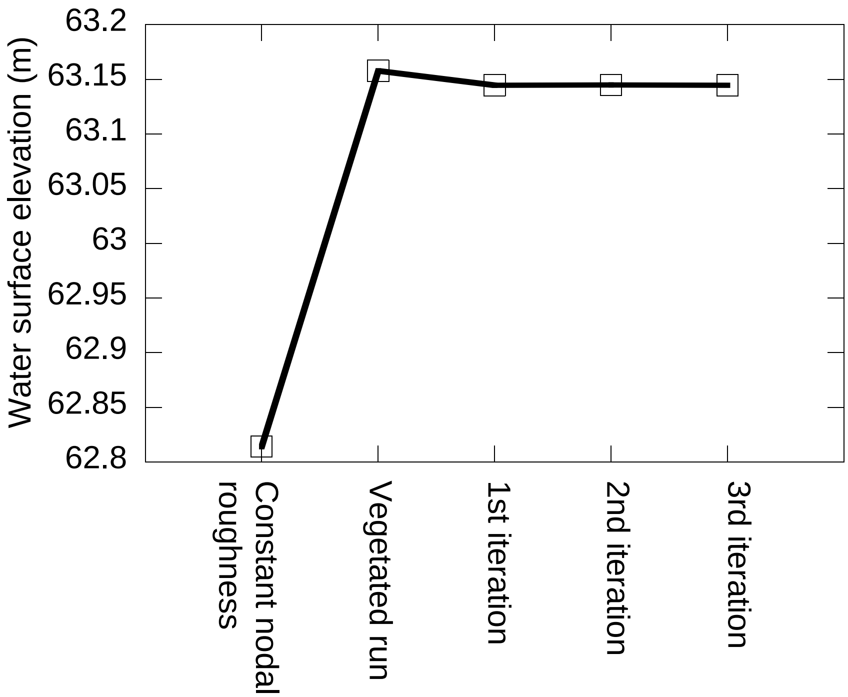

Water surface elevation (m)
63.2
63.15
63.1
63.05
63
62.95
62.9
62.85
62.8
Constant nodal roughness
Vegetated run
1st iteration
2nd iteration
3rd iteration

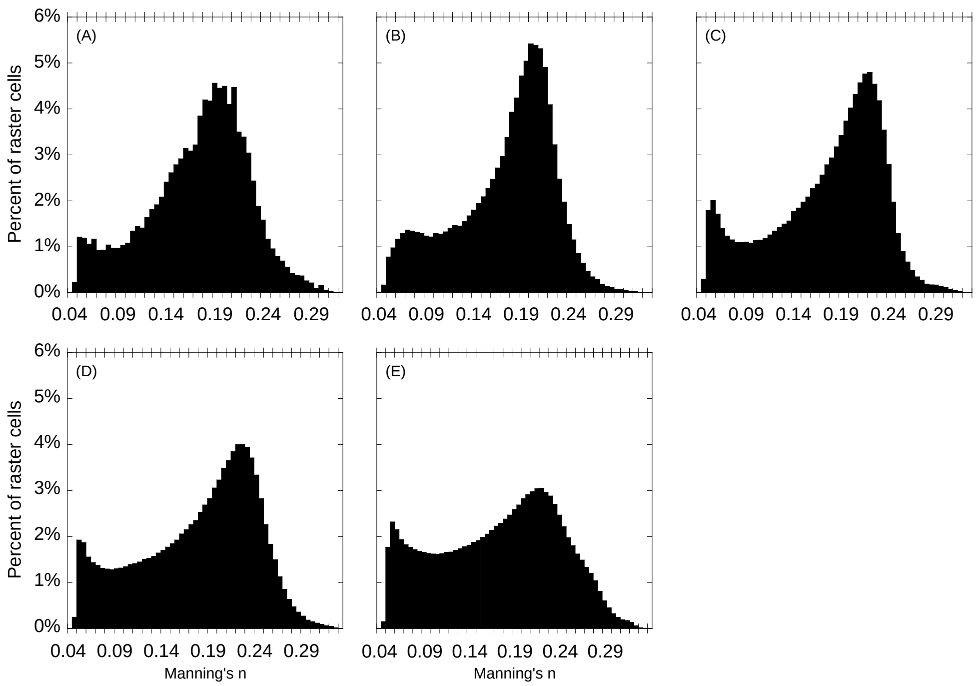

(A)
(B)
(C)
(D)
(E)
Percent of raster cells
0%
1%
2%
3%
4%
5%
6%
0.04
0.09
0.14
0.19
0.24
0.29
Manning's n

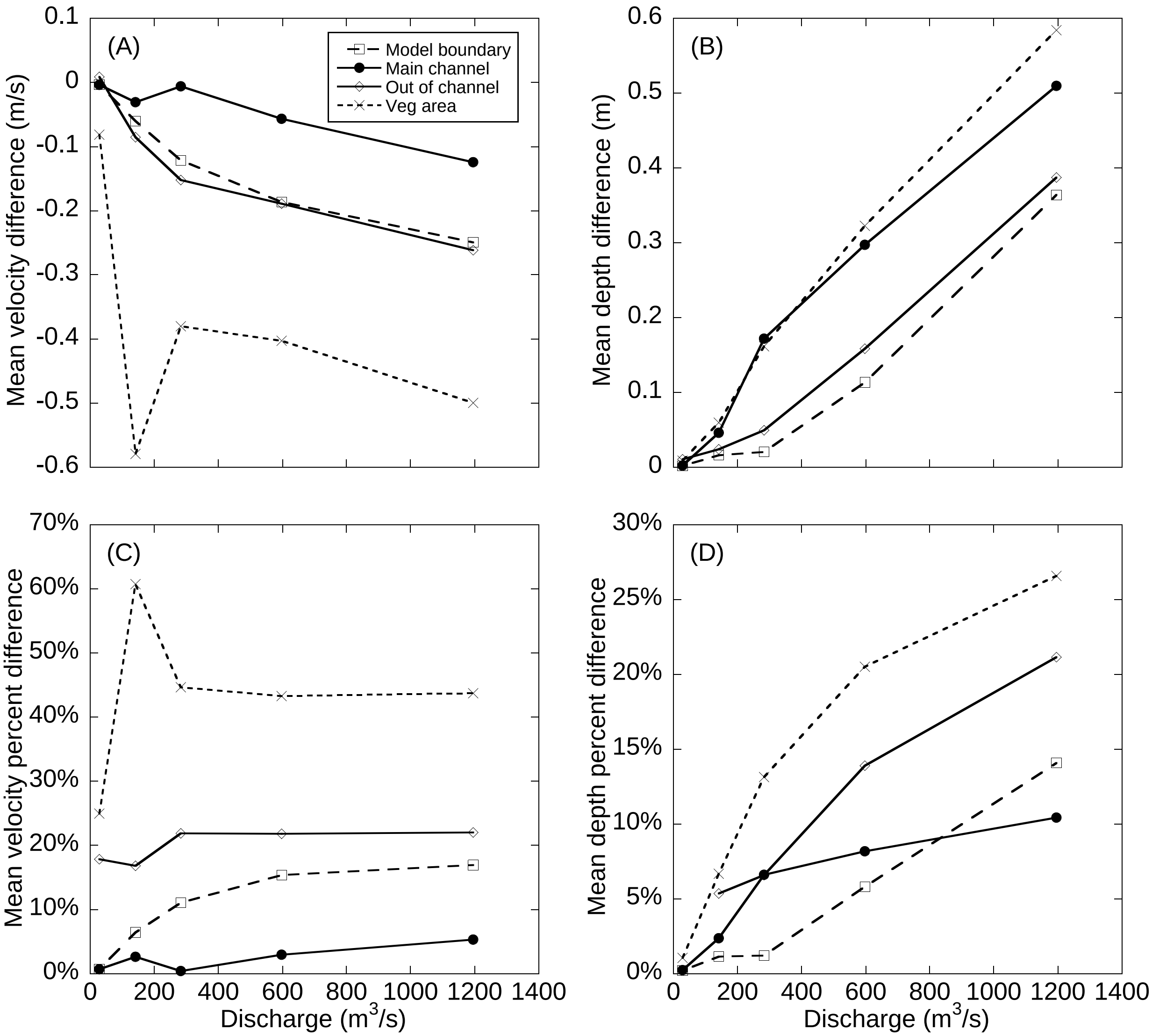

(A)
(B)
(C)
(D)
Model boundary
Main channel
Out of channel
Veg area
Mean velocity difference (m/s)
Mean depth difference (m)
Mean velocity percent difference
Mean depth percent difference
Discharge (m^3/s)

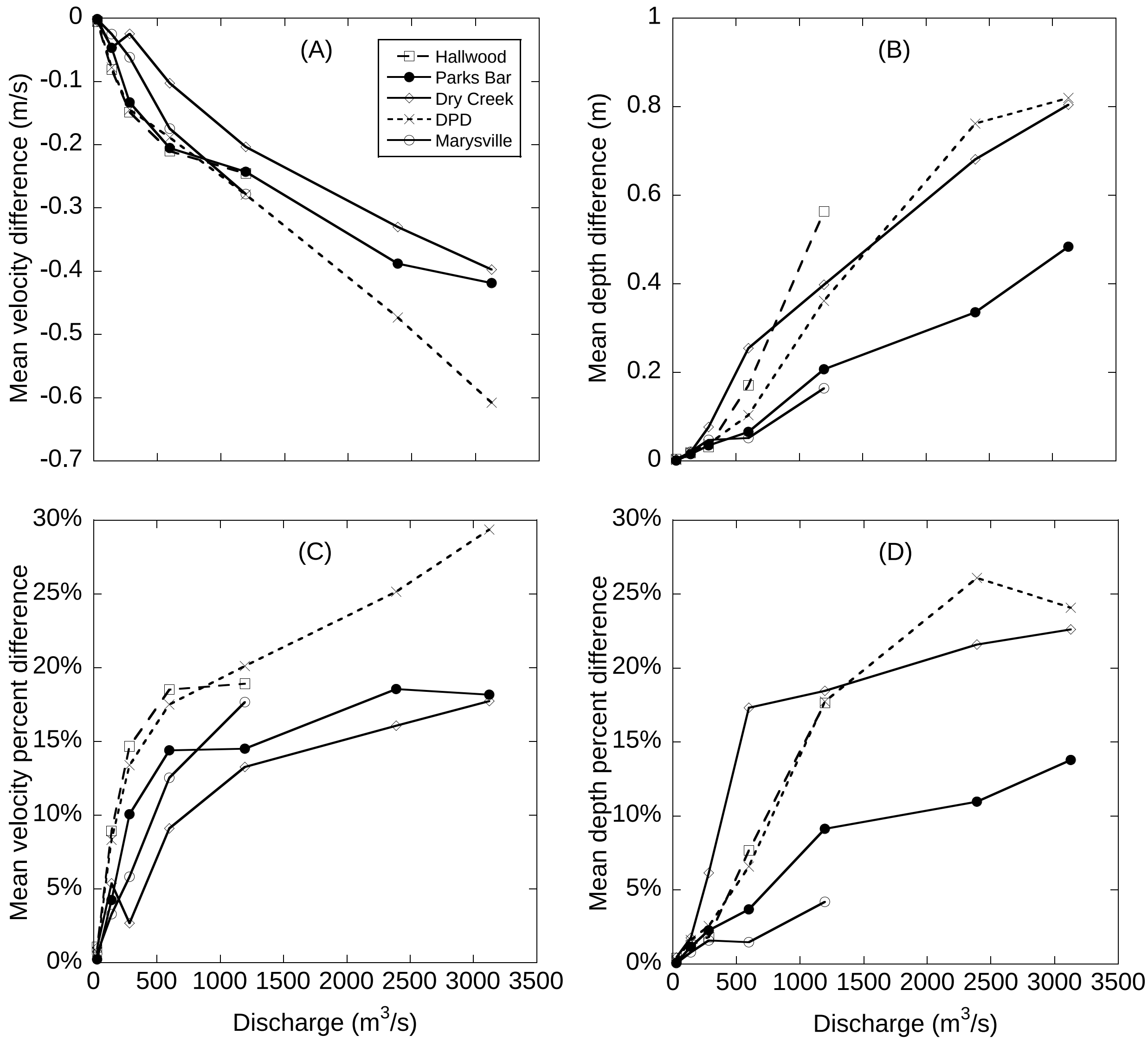
(A)
(B)
(C)
(D)
Hallwood
Parks Bar
Dry Creek
DPD
Marysville
Mean velocity difference (m/s)
Mean depth difference (m)
Mean velocity percent difference
Mean depth percent difference
Discharge (m3/s)
0
-0.1
-0.2
-0.3
-0.4
-0.5
-0.6
-0.7
1
0.8
0.6
0.4
0.2
0
30%
25%
20%
15%
10%
5%
0%
0 500 1000 1500 2000 2500 3000 3500

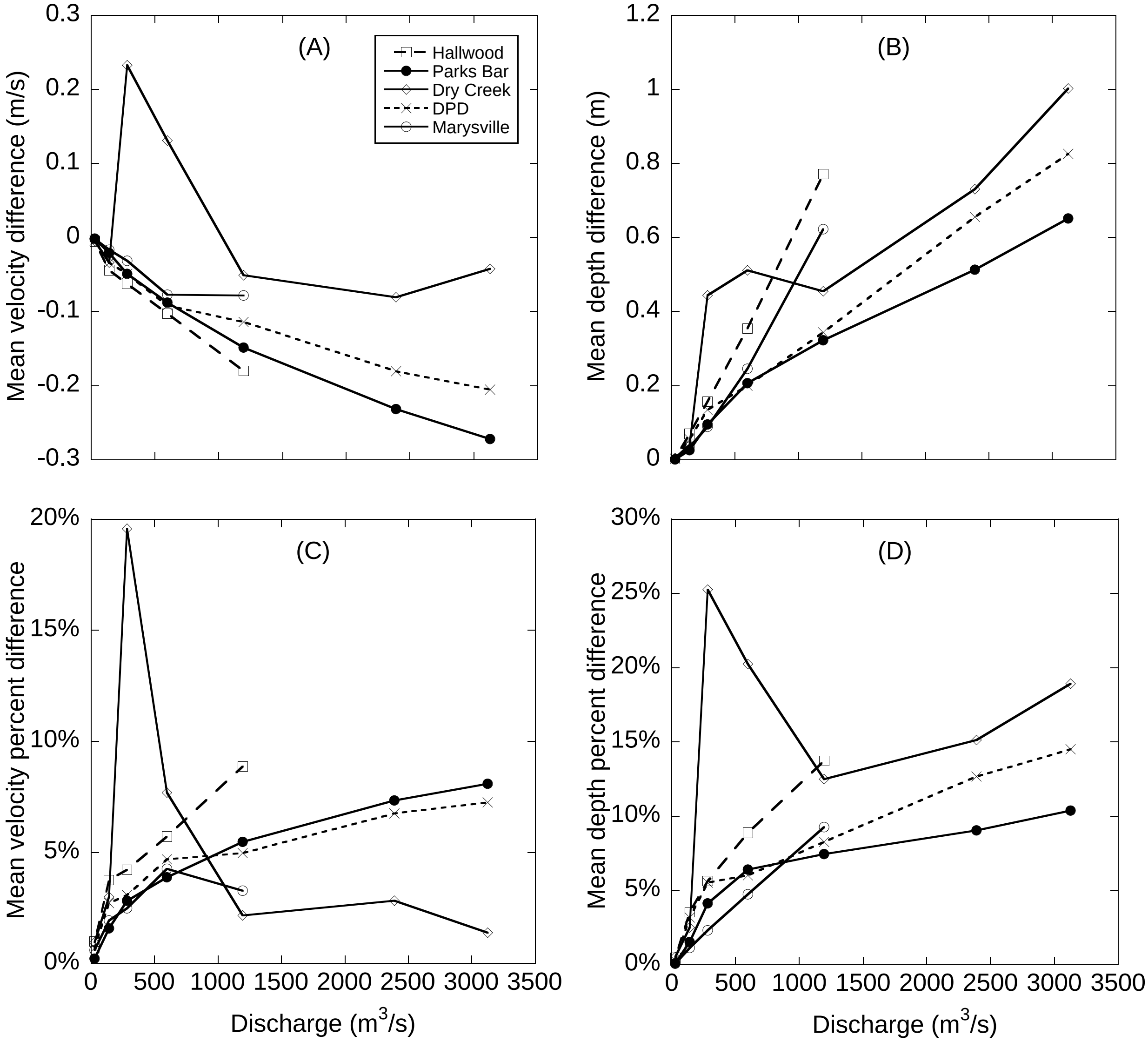
(A)
(B)
(C)
(D)
Hallwood
Parks Bar
Dry Creek
DPD
Marysville
Mean velocity difference (m/s)
Mean depth difference (m)
Mean velocity percent difference
Mean depth percent difference
Discharge (m3/s)
Discharge (m3/s)

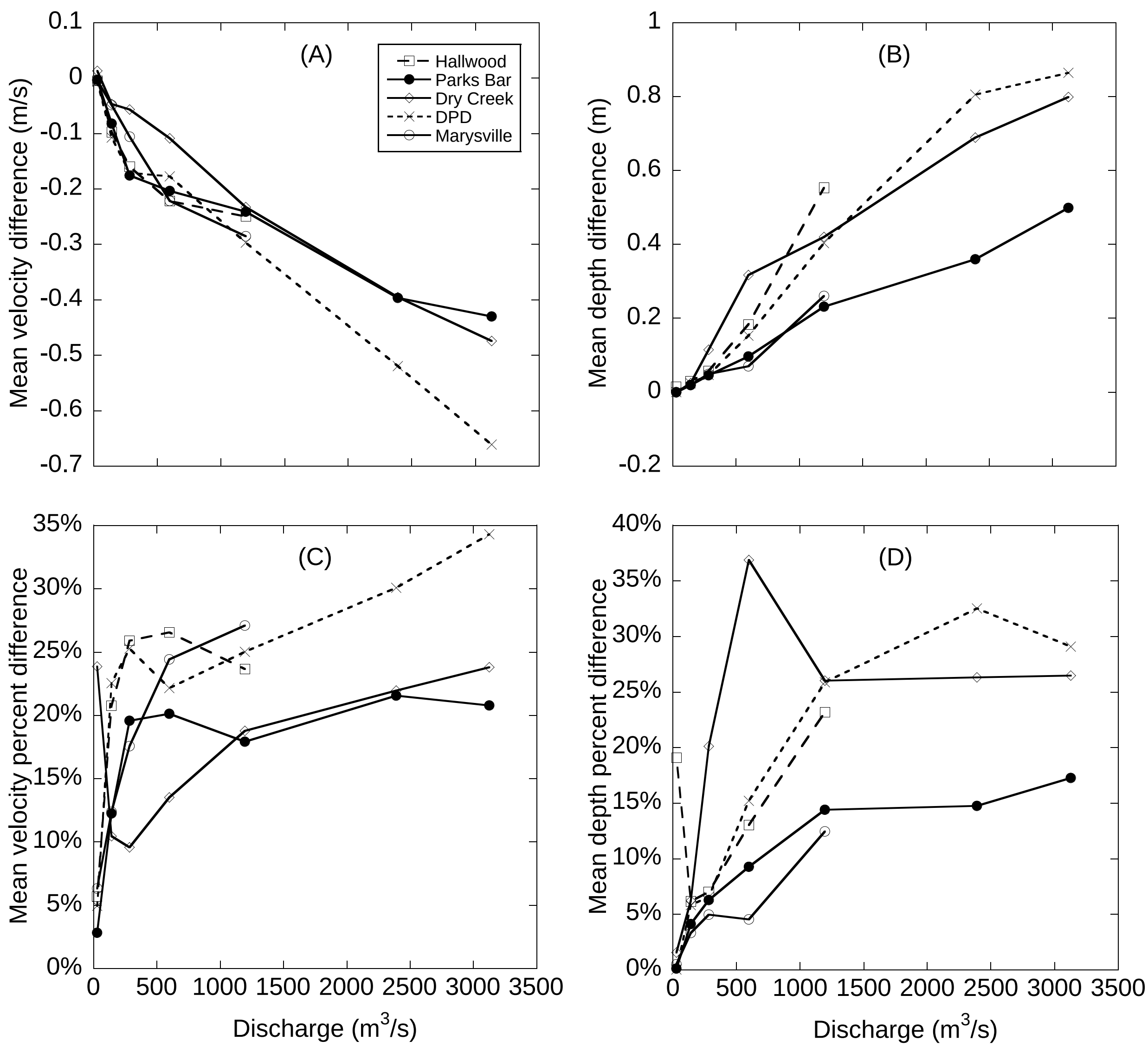
(A)
(B)
(C)
(D)
Hallwood
Parks Bar
Dry Creek
DPD
Marysville
Mean velocity difference (m/s)
Mean depth difference (m)
Mean velocity percent difference
Mean depth percent difference
Discharge (m^3/s)
Discharge (m^3/s)

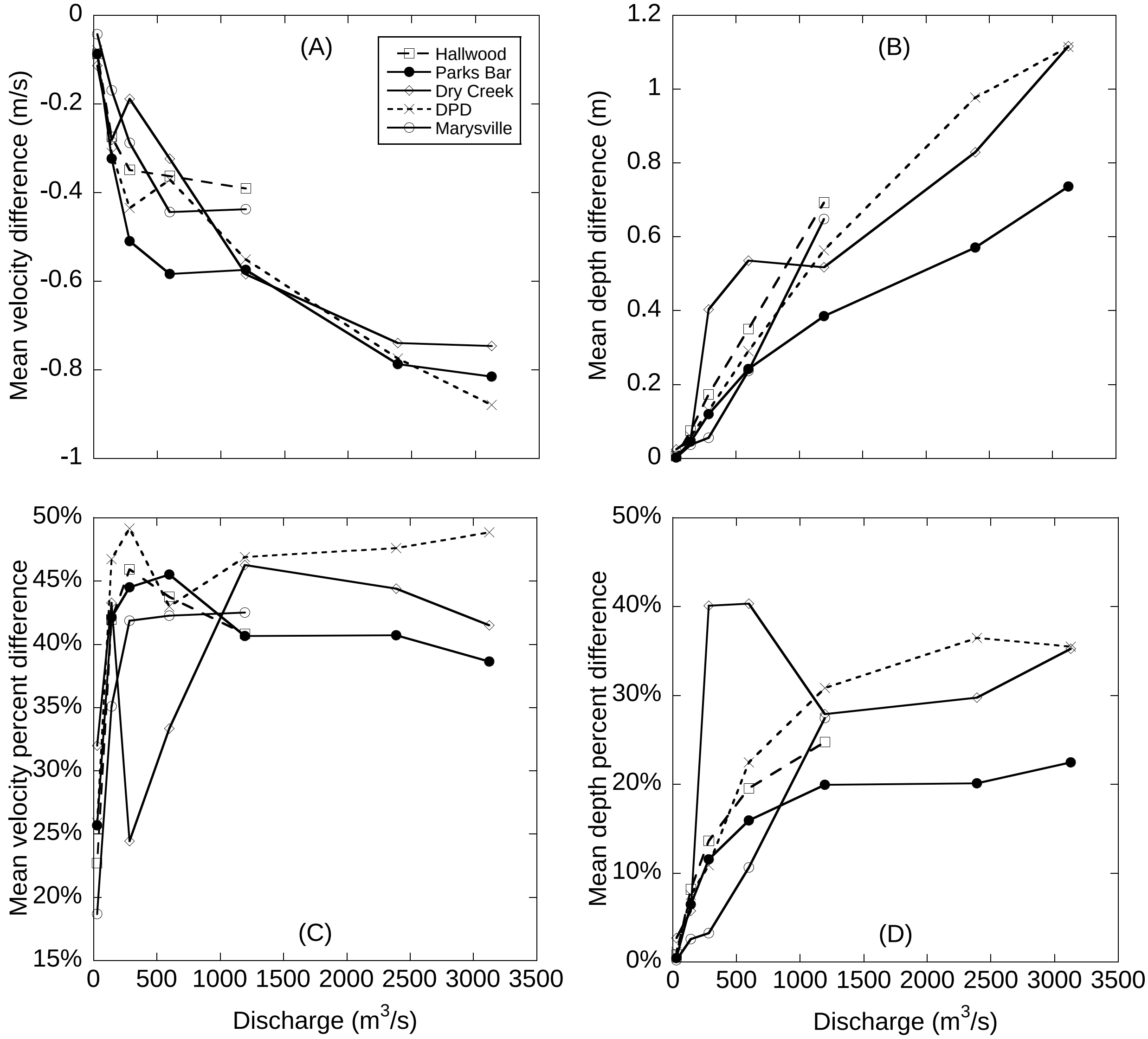
(A)
(B)
(C)
(D)
Hallwood
Parks Bar
Dry Creek
DPD
Marysville
Mean velocity difference (m/s)
Mean depth difference (m)
Mean velocity percent difference
Mean depth percent difference
Discharge (m3/s)
0
-0.2
-0.4
-0.6
-0.8
-1
1.2
1
0.8
0.6
0.4
0.2
50%
45%
40%
35%
30%
25%
20%
15%
10%
0%
500
1000
1500
2000
2500
3000
3500

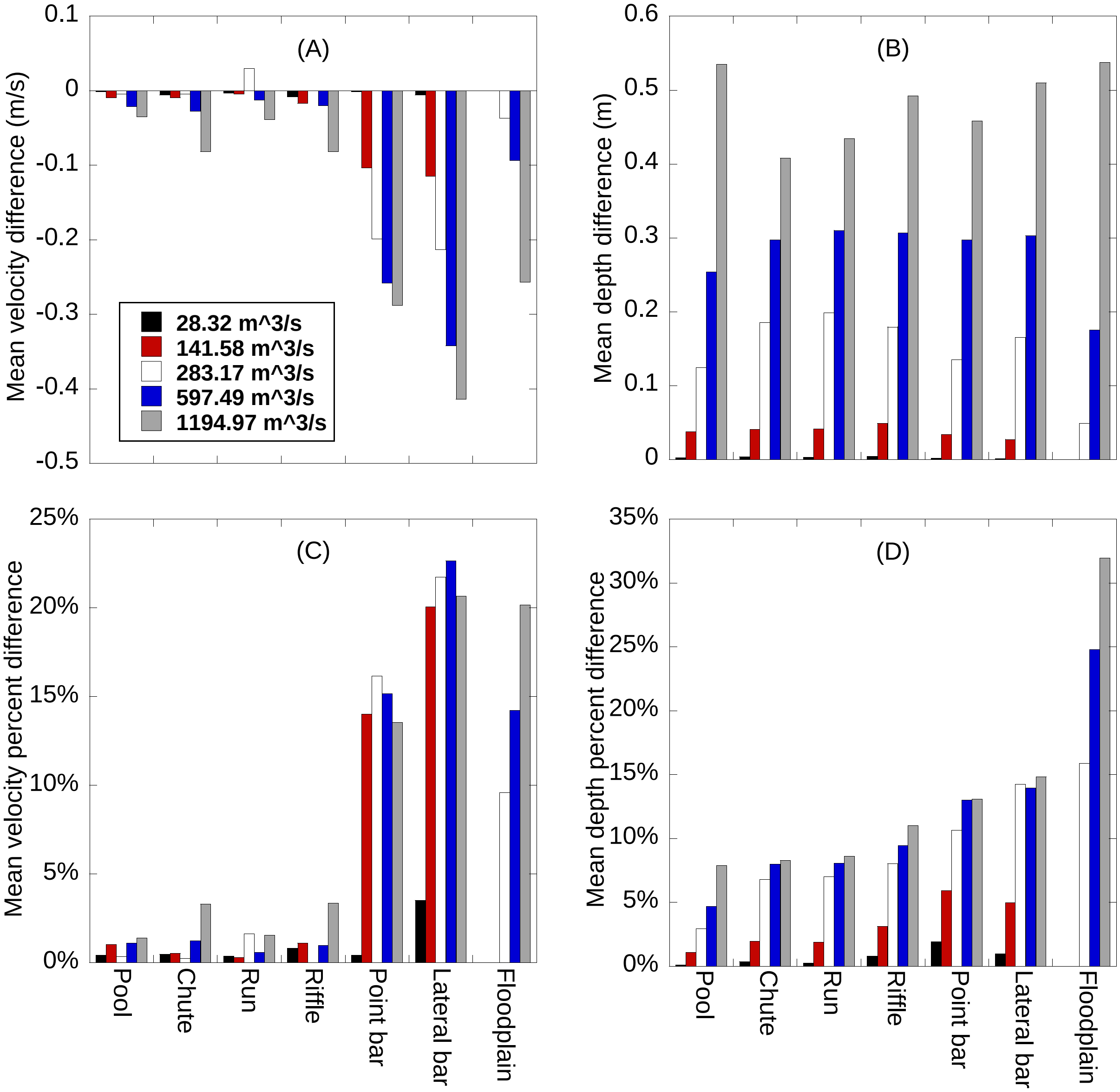

(A)
(B)
(C)
(D)
Mean velocity difference (m/s)
Mean depth difference (m)
Mean velocity percent difference
Mean depth percent difference
28.32 m^3/s
141.58 m^3/s
283.17 m^3/s
597.49 m^3/s
1194.97 m^3/s
0.1
0
-0.1
-0.2
-0.3
-0.4
-0.5
0.6
0.5
0.4
0.3
0.2
0.1
0
25%
20%
15%
10%
5%
0%
35%
30%
25%
20%
15%
10%
5%
0%
Pool
Chute
Run
Riffle
Point bar
Lateral bar
Floodplain

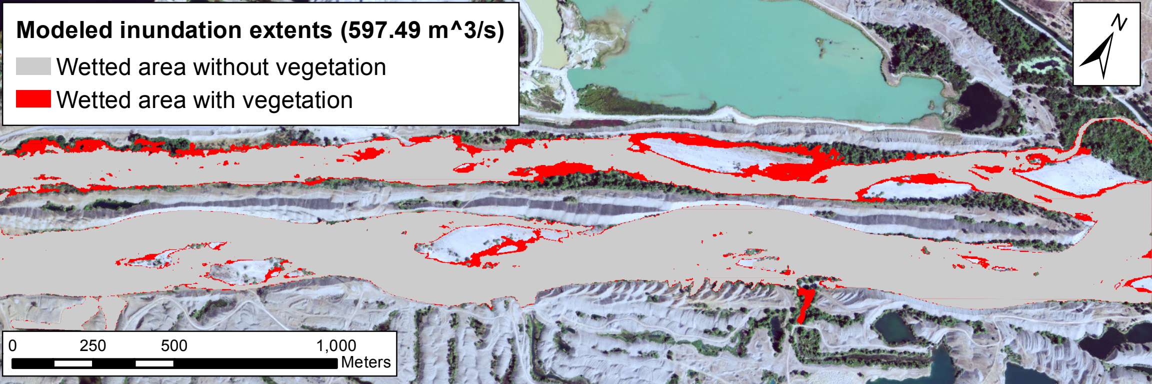
Modeled inundation extents (597.49 m^3/s)
Wetted area without vegetation
Wetted area with vegetation
N
0
250
500
1,000
Meters

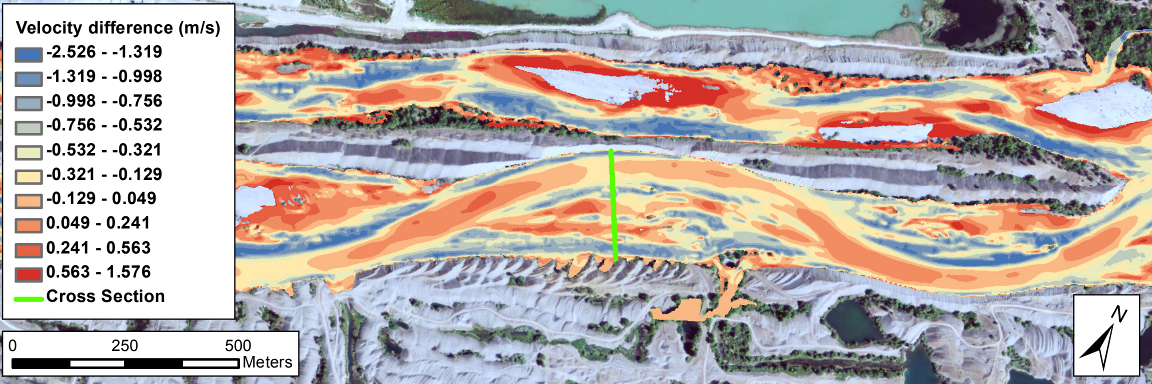
Velocity difference (m/s)
-2.526 - -1.319
-1.319 - -0.998
-0.998 - -0.756
-0.756 - -0.532
-0.532 - -0.321
-0.321 - -0.129
-0.129 - 0.049
0.049 - 0.241
0.241 - 0.563
0.563 - 1.576
Cross Section
0
250
500
Meters
N

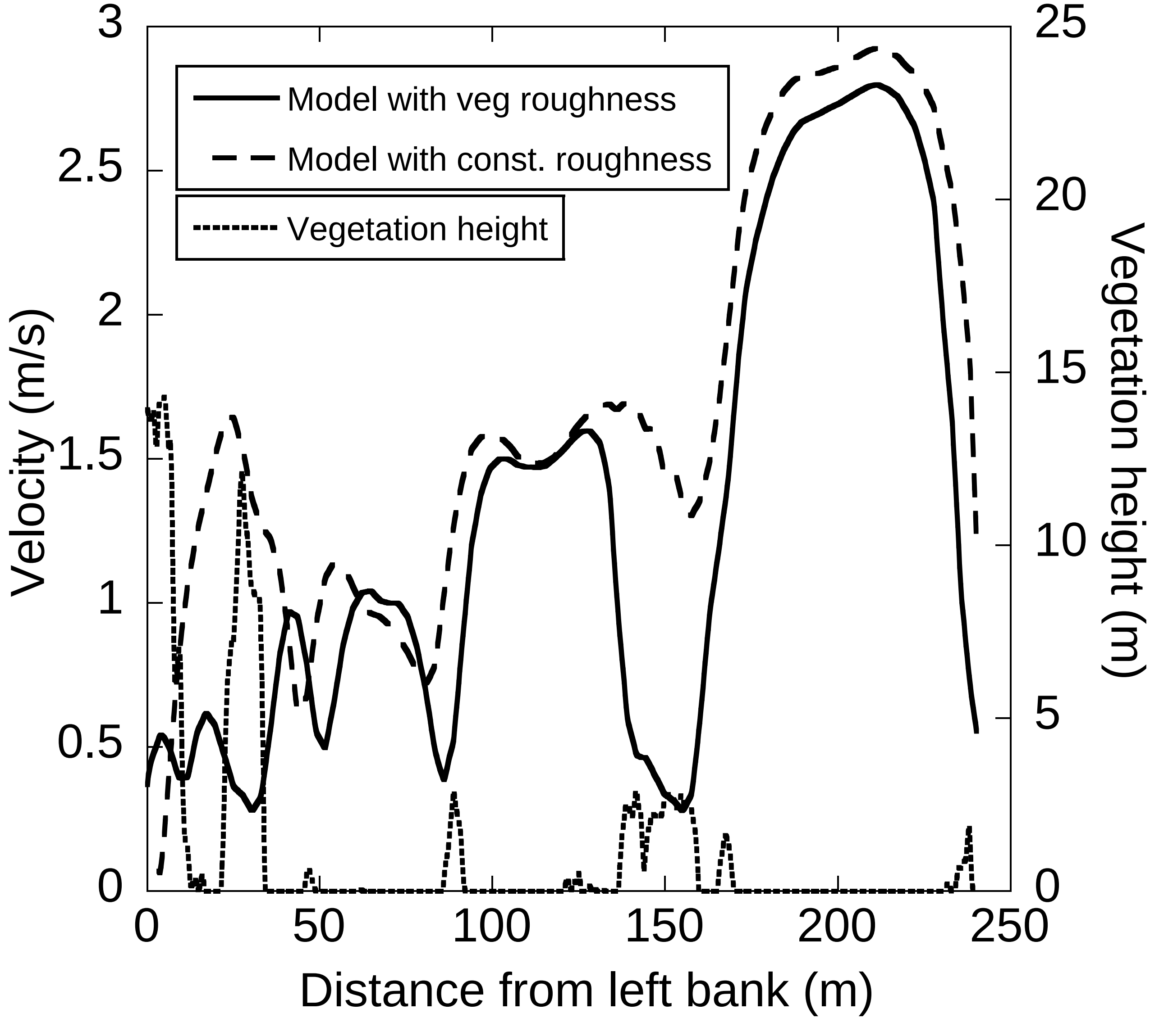

Model with veg roughness
Model with const. roughness
Vegetation height
Velocity (m/s)
Vegetation height (m)
Distance from left bank (m)
0
0.5
1
1.5
2
2.5
3
5
10
15
20
25
50
100
150
200
250

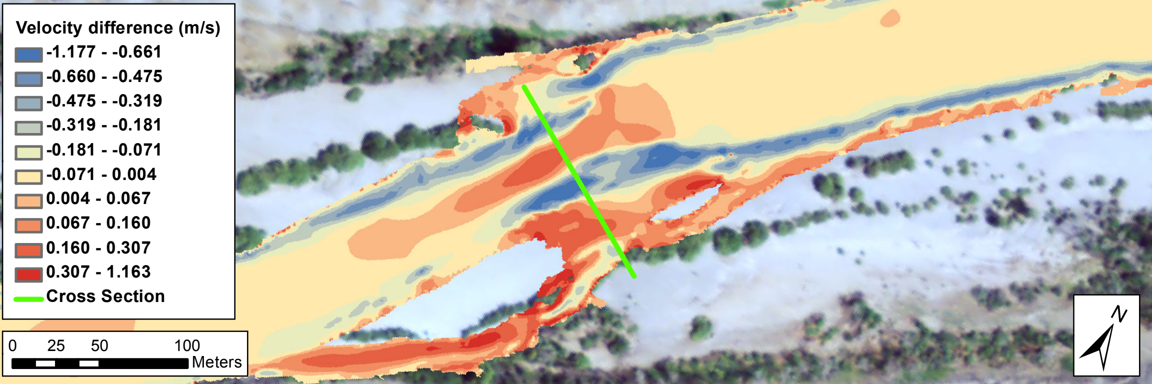
Velocity difference (m/s)
-1.177 - -0.661
-0.660 - -0.475
-0.475 - -0.319
-0.319 - -0.181
-0.181 - -0.071
-0.071 - 0.004
0.004 - 0.067
0.067 - 0.160
0.160 - 0.307
0.307 - 1.163
Cross Section
0 25 50 100
Meters
N

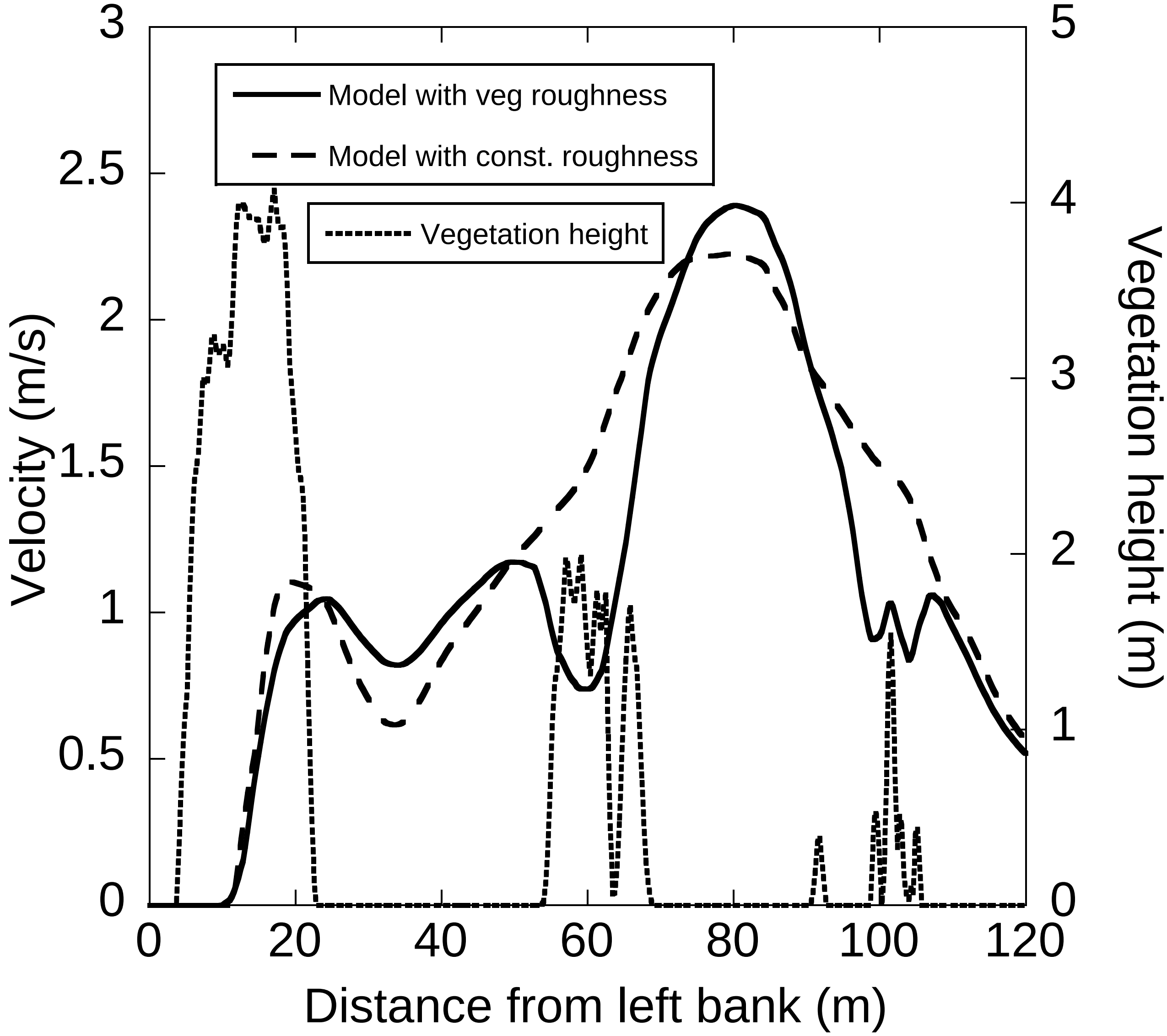

Model with veg roughness
Model with const. roughness
Vegetation height
Velocity (m/s)
Vegetation height (m)
Distance from left bank (m)
0
0.5
1
1.5
2
2.5
3
0
1
2
3
4
5
0
20
40
60
80
100
120